Computation of leaky waves in layered structures coupled to unbounded media by exploiting multiparameter eigenvalue problems

Hauke Gravenkamp [a], Bor Plestenjak [b], Daniel A. Kiefer [c], Elias Jarlebring [d],*

[a] *International Centre for Numerical Methods in Engineering (CIMNE), 08034 Barcelona, Spain*
[b] *IMFM and Faculty of Mathematics and Physics, University of Ljubljana, Jadranska 19, SI-1000 Ljubljana, Slovenia*
[c] *Institut Langevin, ESPCI Paris, Université PSL, CNRS, 75005 Paris, France*
[d] *Department of Mathematics, NA group, KTH Royal Institute of Technology, 100 44 Stockholm, Sweden*

ARTICLE INFO

ABSTRACT

We present a semi-analytical approach to compute quasi-guided elastic wave modes in horizontally layered structures radiating into unbounded fluid or solid media. This problem is of relevance, e.g., for the simulation of guided ultrasound in embedded plate structures or seismic waves in soil layers over an elastic half-space. We employ a semi-analytical formulation to describe the layers, thus discretizing the thickness direction by means of finite elements. For a free layer, this technique leads to a well-known quadratic eigenvalue problem for the mode shapes and corresponding horizontal wavenumbers. Incorporating the coupling conditions to account for the adjacent half-spaces gives rise to additional terms that are nonlinear in the wavenumber. We show that the resulting nonlinear eigenvalue problem can be cast in the form of a multiparameter eigenvalue problem whose solutions represent the wave numbers in the plate and in the half-spaces. The multiparameter eigenvalue problem is solved numerically using recently developed algorithms. Matlab implementations of the proposed methods are publicly available.

1. Introduction

One of the classical problems in elastodynamics is the description of wave propagation in elastic layers that are in contact with another medium of infinite extent at one or both surfaces. We present a computational approach for this problem in the setting where the unbounded domains are assumed homogeneous and consist either of an acoustic fluid (i.e., governed by the scalar wave equation) or a linearly elastic isotropic solid. Such configurations are frequently encountered, particularly in two different fields of engineering: In soil dynamics and earthquake engineering, the analysis of wave propagation and vibration in layered soils and rock formations is of interest, where it can often be assumed that the layers radiate energy into a much larger domain of, e.g., water or soil [1,2]. In this field of study, large structures and small frequencies are typically encountered. At very different spatial and temporal scales, understanding the behavior of high-frequency guided waves in thin-walled structures immersed or embedded in other media is essential in the context of ultrasonic nondestructive testing, material characterization, or sensor development [3–5].

For the modeling of waves in layered media, numerous analytical, numerical, and semi-analytical approaches have been developed. Analytical and semi-analytical methods are appropriate for obtaining dispersion curves of guided and quasi-guided

---

waves, which will be the focus of the present work. Wave propagation in individual layers with traction-free or fixed surfaces is well-understood, and implicit closed-form expressions for their dispersion relations are available [6,7]. However, obtaining from these relations all solutions at a given frequency already requires sophisticated numerical root-finding algorithms. Extensions to layered systems and their coupling to unbounded domains have been achieved by means of the Transfer Matrix Method, Global Matrix Method, or Stiffness Matrix Method [8–10]. However, in such cases, the numerical difficulties in obtaining all solutions as roots of the dispersion relations are significant. For this reason, semi-analytical methods have been established as effective means of describing waves in plates and other structures of constant cross-section [11]. These approaches involve a discretization of the structure's cross-section, which, in the case of layered media in two dimensions, reduces to a one-dimensional discretization along the layer's thickness. Typically, standard finite element spaces are employed to this end [12–14], while variants based on, e.g., non-uniform rational B-splines (NURBS) [15] or spectral collocation [16] exist. Such formulations naturally lead to a quadratic eigenvalue problem, whose solutions represent wavenumbers and discretized mode shapes and can be solved robustly and efficiently using conventional algorithms. To researchers in soil dynamics, this concept of semi-discretization is most famously known as Thin Layer Method (TLM) [17], while, in the context of ultrasonic testing, the term Semi-Analytical Finite Element Method (SAFE) [18] is common. Furthermore, the Scaled Boundary Finite Element Method (SBFEM) has been developed and expanded since the 1990s [19–21] with the aim of extending the range of application of semi-analytical methods. The SBFEM has its origins in the TLM but introduced a particular coordinate transformation in order to employ the semi-analytical concepts to more general bounded and unbounded star-convex domains.

Notwithstanding the efficiency and robustness of semi-analytical methods for modeling waveguides of arbitrary cross-sections, incorporating an adjacent unbounded domain coupled to the structure of interest is not straightforward. Consequently, a variety of formulations have been suggested to address this challenge. An obvious idea is to discretize a finite part of the unbounded domain large enough to allow waves to decay sufficiently such that reflections of the computational domain's boundary cannot interfere with the waveguide modes. These approaches require artificial damping in the unbounded domain, which is often achieved either by classical absorbing regions with artificial viscoelastic damping [22] or coordinate mapping techniques such as perfectly matched layers (PML) [23–25], infinite elements [26,27], or similar approaches based on a problem-adapted complex coordinate scaling [28,29]. Still, the discussed discretizations increase the number of unknowns, and choosing suitable damping properties is not always straightforward. Furthermore, they require distinguishing between those modes propagating in the waveguide and those excited primarily within the damped medium. Hence, it is desirable to describe the effect of the unbounded domain on the waveguide solely by an interface condition, avoiding the additional discretization and the associated set of nonphysical parameters.

A particularly simple attempt at achieving this goal relies on approximating the effect of an unbounded domain by linear damping (*dashpot* boundary condition) [30,31]. The implied assumption is that waves are radiated in the direction normal to the waveguide's surface into the surrounding medium, which can be a reasonable approximation, depending on the combination of material parameters and the frequency range. On the other hand, incorporating the exact boundary conditions representing the unbounded domain in a rigorous way gives rise to additional *nonlinear* terms in the eigenvalue problem. For the plane geometries considered here, these nonlinear terms are typically of the form

$$\kappa_y = \sqrt{\kappa^2 - k^2}, \tag{1}$$

relating a vertical wavenumber κ_y in the unbounded medium to the common horizontal wavenumber k (i.e., the eigenvalue), with some constant κ. In the case of an adjacent fluid medium, an iterative solution scheme has been devised, which starts from the linear dashpot approximation and iteratively corrects each modal solution by updating the dependency of the fluid coupling on the wavenumber in the structure [32]. This approach is relatively efficient but not always robust, as different starting values may converge to the same solution, resulting in missing modes in the spectrum. Moreover, the trapped waves (quasi-Scholte modes) that appear as additional solutions compared to the free plate are not always found. For the special case of a solid plate in contact with a fluid on one side or the same fluid on both sides, Kiefer et al. [33,34] showed that the eigenvalue problem can be linearized by a change of variables. This approach robustly finds the full spectrum but cannot be generalized to other cases. Hayashi et al. found solutions for the same special case by exploiting symmetries in the wave propagation that enabled the linearization of the problem [35]. More recently, Tang et al. [36] and Ducasse and Deschamps [37] independently presented linearization methods that consist in introducing a higher-dimensional state space. The latter studies consider two different fluids on both sides of the plate.

For more general setups, including layers embedded in solid media or coupled to different materials on both sides, the solution becomes challenging due to the presence of different modes in the unbounded media. In this paper, we will derive the coupling conditions between elastic plates and unbounded fluid or solid media. To describe the plate, we employ a semi-analytical finite element method with high-order Lagrange elements (as discussed in [14,38]) in order to keep the size of the resulting eigenvalue problem to a minimum. A fluid half-space is described by only one additional degree of freedom (DOF) representing the pressure at the interface. In the case of a solid half-space, we use displacement amplitudes at the interface, hence adding two or three degrees of freedom (depending on whether we include shear-horizontal modes) for each unbounded domain.

Due to the incorporation of coupling conditions such as (1) and more complex relations given in Sections 3 and 4, the discretized problem is a nonlinear eigenvalue problem (NLEVP) in the sense of [39]. The solution of such problems is an active research field, particularly in the scope of numerical linear algebra, with a plentitude of algorithms for general problems as well as approaches tailored to specialized structures [40], including those that arise in the modeling of waveguides [41]. Algorithms and methods have also been included in software packages for high-performance computing such as SLEPc (*Scalable Library for Eigenvalue Problem Computations*) [42].
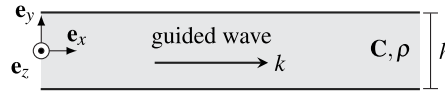
Fig. 1. Plate with traction-free surfaces.

For the particular type of nonlinearity encountered in the current work, we employ a rather different technique based on a relationship between certain NLEVPs and multiparameter eigenvalue problems, as formally defined below. The general connection was pointed out in a presentation by M. Shao[1] and has been exploited to develop methods for such problems in [43]. We will demonstrate that the nonlinear eigenvalue problem addressed here can be cast into the form of a multiparameter eigenvalue problem, in which the vertical wavenumbers of the form κ_y are interpreted as additional unknown parameters related to the eigenvalue k through (in the case of fluid loading) Eq. (1), or slightly different relations in the case of coupling to a solid medium.

Generally, in a multiparameter eigenvalue problem [44], we have r equations of the form

$$(\mathbf{A}_{i0} + \lambda_1 \mathbf{A}_{i1} + \cdots + \lambda_r \mathbf{A}_{ir}) \mathbf{x}_i = \mathbf{0}, \qquad i = 1, \ldots, r, \tag{2}$$

where $\mathbf{A}_{ij}$ is an $n_i \times n_i$ matrix. Eigenvalues are tuples $(\lambda_1, \ldots, \lambda_r)$ for which nonzero $\mathbf{x}_i$ exist such that all equations are satisfied. Problems of this type also appear, e.g., in separable boundary-value problems [45]. Recently, this formalism was applied to the computation of zero-group-velocity (ZGV) points in waveguides [16]. A standard numerical approach to computing all eigenvalues consists in constructing the associated system of generalized eigenvalue problems $\mathbf{\Delta}_i \mathbf{z} = \lambda_i \mathbf{\Delta}_0 \mathbf{z}$, $i = 1, \ldots, r$; for details see Appendix B. The latter system has the same eigenvalues $(\lambda_1, \ldots, \lambda_r)$ as the original problem but can now be solved with conventional methods [46], since the r equations decouple in the eigenvalues. If the problem is singular, the regular part is first extracted using a staircase-type method [47].

Our proposed approach is implemented in Matlab, making use of the toolbox MultiParEig [48] for the solution of multiparameter eigenvalue problems. The codes for reproducing the examples discussed in this paper are available for download [49]. We also incorporated this method in the toolbox SAMWISE [50], which allows applying this algorithm to user-defined problems.

In the following section, we briefly recap the semi-analytical formulation of a free plate and state the general form of the nonlinear eigenvalue problem resulting from including coupling conditions at the interfaces. Sections 3 and 4 explain the interface conditions for unbounded fluid and elastic media, respectively. The solution of the nonlinear eigenvalue problems is discussed in Section 5, before we present some numerical examples (Section 6) and a conclusion (Section 7).

2. Semi-analytical model of a layered medium

2.1. Free plate

The basic semi-analytical description of waves in a free elastic plate is well-known [12–14], and various implementations are available, e.g., [50,51]. Hence, the concept is only briefly recapitulated here. As depicted in Fig. 1, let the plate of thickness h occupy the domain Ω, defined by the open interval $\mathcal{I} = (-\frac{h}{2}, \frac{h}{2})$ such that

$$\Omega = \left\{ (x, y) \in \mathbb{R}^2 \mid x \in \mathbb{R}, \ y \in \mathcal{I} \right\}.$$

Assuming the linearized momentum equation of elasticity, the displacement field $\overline{\mathbf{u}}(x, y, t)$ in the plate is governed by

$$\nabla \cdot (\mathbf{C} : \nabla \overline{\mathbf{u}}) - \rho \partial_{tt} \overline{\mathbf{u}} = \mathbf{0} \tag{3}$$

with the mass density ρ and stiffness tensor $\mathbf{C}$. Here, ∂_{tt} denotes the second partial derivative with respect to time and ':' the double contraction of two tensors. Consider harmonic wave propagation along x with a wavenumber k and frequency ω, i.e.,[2]

$$\overline{\mathbf{u}}(x, y, t) = \mathbf{u}(k, y, \omega) \, e^{i(kx - \omega t)}. \tag{4}$$

Substituting Eq. (4) into (3), dividing by $e^{i(kx - \omega t)}$, and introducing traction-free boundary conditions,[3] the following one-dimensional boundary-value problem can be stated. For a given ω, find $(k, \mathbf{u})$ such that [34]

$$\left[(ik)^2 \mathbf{C}_{xx} + ik\, \mathbf{C}_{xy} \partial_y + ik\, \mathbf{C}_{yx} \partial_y + \mathbf{C}_{yy} \partial_y^2 + \omega^2 \rho \mathbf{I} \right] \mathbf{u} = \mathbf{0}, \qquad y \in \mathcal{I} \tag{5a}$$

$$\left[ik \mathbf{C}_{yx} + \mathbf{C}_{yy} \partial_y \right] \mathbf{u} = \mathbf{0}, \qquad y = \pm \frac{h}{2} \tag{5b}$$

---

[1] M. Shao, Conquering algebraic nonlinearity in nonlinear eigenvalue problems, presented at the SIAM Conference on Applied Linear Algebra (ALA), Hong Kong 2018; joint work with Z. Bai, W. Gao, and X. Huang.

[2] Throughout this paper, we use $\overline{\mathbf{u}}$ to denote the displacement field and a simple $\mathbf{u}$ for the amplitude defined by Eq. (4).

[3] The typical traction-free von-Neumann boundary conditions are assumed here for notational convenience, while we may, alternatively, introduce Dirichlet conditions at the plate's surfaces.

with the 2nd-order tensors $\mathbf{C}_{ij} = \mathbf{e}_i \cdot \mathbf{C} \cdot \mathbf{e}_j$ and the direction vectors $\mathbf{e}_i, i \in \{x, y, z\}$.[4] We can now employ standard finite-element procedures to solve this boundary-value problem [52], i.e., we pose the weak form of Eq. (5a) and subsequently apply discretization. We denote by $\mathcal{W} = \mathbf{H}^1(\Omega)$ the function space of the continuous problem with the standard notation for Sobolev spaces. Multiplying Eq. (5a) by test functions $\mathbf{v} \in \mathcal{W}$ (i.e., taken from the same space as $\mathbf{u}$), integrating over $\mathcal{I}$, and applying integration by parts to the third and fourth term yields the variational statement

$$-k^2\big(\mathbf{v}, \mathbf{C}_{xx}\mathbf{u}\big) + \mathrm{i}k\big(\mathbf{v}, \mathbf{C}_{xy}\partial_y\mathbf{u}\big) - \mathrm{i}k\big(\partial_y\mathbf{v}, \mathbf{C}_{yx}\mathbf{u}\big) - \big(\partial_y\mathbf{v}, \mathbf{C}_{yy}\partial_y\mathbf{u}\big) + \omega^2\big(\mathbf{v}, \rho\mathbf{u}\big) = \mathbf{0}, \tag{6}$$

where $(\cdot, \cdot)$ denotes the L^2-inner product in $\mathcal{I}$. The weak form (6) is discretized straightforwardly by defining adequate finite element spaces $\mathcal{W}_h \subset \mathcal{W}$. Replacing the trial and test functions in (6) with the discrete counterparts $\mathbf{u}_h, \mathbf{v}_h \in \mathcal{W}_h$ defines the discretized boundary-value problem. Performing the integrations numerically, one obtains a square matrix for each of the terms in (6), denoted as

$$\big(-k^2\,\mathbf{E}_0 + \mathrm{i}k\,\mathbf{E}_1 - \mathbf{E}_2 + \omega^2\,\mathbf{M}\big)\,\mathbf{u}_n = \mathbf{0}. \tag{7}$$

Here, $\mathbf{u}_n$ refers to the vector of coefficients of the finite element discretization, which, in our case, are nodal displacements. Explicit expressions for computing these matrices are given in Appendix A. Eq. (7) relates frequencies and horizontal wavenumbers, which implicitly defines a dispersion relation. This equation poses a quadratic two-parameter eigenvalue problem that is commonly solved by choosing a set of frequencies and computing the corresponding wavenumbers after employing a companion linearization.

Remark 1. In the case of undamped free plates or similarly simple scenarios, we can alternatively obtain dispersion curves by choosing a set of real wavenumbers and computing the corresponding frequencies. This can be computationally cheaper, as Eq. (7) directly poses a linear eigenvalue problem for ω^2. However, in the case of material damping or radiation into adjacent media, the wavenumbers of interest are complex; hence, we must solve Eq. (7) at given frequencies, which we know to lie on a real interval.

Remark 2. In finite-element-based formulations like the one outlined above, it is straightforward to incorporate any anisotropic material behavior of the plate into the stiffness tensor, see, e.g., [14,53]. On the other hand, when dealing with elastic half-spaces (Section 4), we will assume those to be isotropic.

Remark 3. We will see that the computational costs for solving the nonlinear eigenvalue problems discussed in the ensuing increase rapidly with the size of the finite-element matrices. Hence, it is crucial to choose an efficient discretization scheme. For this purpose, it is highly beneficial to use as few elements as possible (in our current application, one element per layer) of an order adequate to obtain reasonably accurate results in the desired frequency range. As has been discussed in much detail previously, a suitable and rather common choice of trial and test functions is provided by Lagrange interpolation polynomials with nodes positioned at the Gauss–Lobatto points, allowing polynomial degrees of 100 and more without numerical issues [14,38,54]. Alternatives can be found in hierarchical shape functions or NURBS [15], leading to similar numerical properties. An overview in the context of the SBFEM is provided in [55].

2.2. General form of the nonlinear EVP

In the following sections, we will see that incorporating the coupling to unbounded domains at the plate's top and bottom surfaces leads to a modified nonlinear eigenvalue problem of the general form

$$\big(-k^2\,\overline{\mathbf{E}}_0 + \mathrm{i}k\,\overline{\mathbf{E}}_1 - \overline{\mathbf{E}}_2 + \omega^2\,\overline{\mathbf{M}} + \mathbf{R}(k)\big)\,\boldsymbol{\phi} = \mathbf{0}. \tag{8}$$

The eigenvector $\boldsymbol{\phi}$ contains the nodal displacements $\mathbf{u}_n$ of the plate and also up to six additional degrees of freedom representing the unbounded domains. The matrix function $\mathbf{R}(k)$ involves non-polynomial terms in the eigenvalue k and incorporates the interaction of the waveguide with a surrounding/adjacent medium. Different approaches can be used to describe the waveguide as well as the surrounding medium. We formulate wave propagation inside elastic media in terms of displacements, while other formulations based on elastic potentials or mixed interpolations are possible. Waves in acoustic media can be defined in terms of the acoustic pressure or the velocity potential (we opt for the former). We also note that it is generally possible to eliminate the degrees of freedom in the unbounded domain and only incorporate their effect on the waveguide through (nonlinear) Neumann boundary conditions as has been done, e.g., in [32]. However, that approach leads to a more complicated dependency of the additional terms in $\mathbf{R}(k)$ on the eigenvalue k and hinders the solution by the approaches that we suggest in the following sections.

3. Elastic plate in contact with a fluid half-space

Let us begin by assuming that the elastic plate, as described in the previous section, is now coupled to an infinite acoustic (inviscid) fluid at one of its surfaces located at $y = y_s$, see Fig. 2. The extension to two (generally different) acoustic half-spaces will

---

[4] For an isotropic medium with the Lamé parameters λ and μ, we have

$$\mathbf{C}_{xx} = \begin{bmatrix} \lambda + 2\mu & 0 & 0 \\ 0 & \mu & 0 \\ 0 & 0 & \mu \end{bmatrix}, \qquad \mathbf{C}_{yy} = \begin{bmatrix} \mu & 0 & 0 \\ 0 & \lambda + 2\mu & 0 \\ 0 & 0 & \mu \end{bmatrix}, \qquad \mathbf{C}_{yx} = \mathbf{C}_{xy}^{\mathrm{T}} = \begin{bmatrix} 0 & \mu & 0 \\ \lambda & 0 & 0 \\ 0 & 0 & 0 \end{bmatrix}.$$
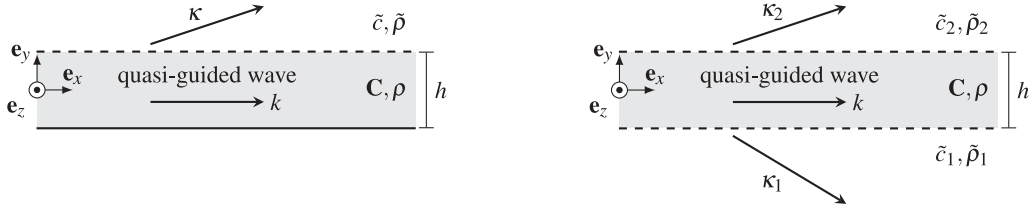
Fig. 2. Plate in contact with fluid half-spaces at one or both of its surfaces.

be straightforward. The acoustic pressure $\bar{p}$ in the fluid satisfies the Helmholtz equation

$$\Delta \bar{p} + \kappa^2 \bar{p} = 0, \tag{9}$$

where κ denotes the wavenumber in the fluid. As we are dealing with a plane surface radiating into an infinite medium, we postulate plane pressure waves [56] of amplitude p propagating in the fluid domain, i.e.,

$$\bar{p}(x, y, t) = p\, \mathrm{e}^{\mathrm{i}(\kappa_x x + \kappa_y y - \omega t)}, \tag{10}$$

with κ_x and κ_y being the horizontal and vertical components of the complex-valued wave vector in the fluid. Assuming continuity of vertical displacements at the interface requires a common horizontal wavenumber in all domains, i.e., $\kappa_x = k$ (cf. Snell's law [56,57]). The vertical wavenumber is then given by

$$\kappa_y = \pm\sqrt{\kappa^2 - k^2}. \tag{11}$$

We absorb the constant $\mathrm{e}^{\mathrm{i}\kappa_y y_s}$ into the complex-valued amplitude $p_s = p\, \mathrm{e}^{\mathrm{i}\kappa_y y_s}$. With this, the fluid pressure along the interface $y = y_s$ reads

$$\bar{p}(x, y_s, t) = p_s\, \mathrm{e}^{\mathrm{i}(kx - \omega t)}. \tag{12}$$

The coupling conditions at the interface are as follows. The acoustic pressure induces a traction $\boldsymbol{\tau}$ on the plate surface, i.e.,

$$\boldsymbol{\tau}(y = y_s) = \mathbf{n} \cdot \boldsymbol{\sigma}(y = y_s) = p_s\, \mathbf{n} \tag{13}$$

with the unit outward normal vector $\mathbf{n}$ and the stress tensor $\boldsymbol{\sigma}$. Since, in our case, we have either $\mathbf{n} = \mathbf{e}_y$ or $\mathbf{n} = -\mathbf{e}_y$, this condition simplifies to

$$\tau_y(y = y_s) = \pm p_s, \tag{14}$$

where the positive/negative sign corresponds to coupling at the upper/lower surface, respectively. The second coupling condition states that the normal derivative of the acoustic pressure is related to the acceleration at the plate's surface by

$$\mathbf{n} \cdot \nabla \bar{p}\big|_{y = y_s} = -\tilde{\rho}\, \mathbf{n} \cdot \partial_t^2 \overline{\mathbf{u}} = \omega^2 \tilde{\rho}\, \mathbf{n} \cdot \overline{\mathbf{u}} \tag{15}$$

with the fluid's density $\tilde{\rho}$. Hence, considering Eqs. (10) and (11), we obtain

$$\pm \mathrm{i}\sqrt{\kappa^2 - k^2}\, p_s = \omega^2 \tilde{\rho}\, u_y(y = y_s). \tag{16}$$

Two possibilities exist for including the coupling conditions in the waveguide model. The first one, described in detail in [32], consists in substituting Eq. (16) into (14) to obtain an expression for the traction while eliminating the acoustic pressure:

$$\tau_y(y = y_s) = \mp \frac{\mathrm{i}\omega^2 \tilde{\rho}}{\sqrt{\kappa^2 - k^2}}\, u_y(y = y_s). \tag{17}$$

The above equation can be considered as a Neumann boundary condition and directly integrated into the waveguide eigenproblem. However, the resulting nonlinear terms of the form $1/\sqrt{\kappa^2 - k^2}$, which are singular at $\kappa = k$, are somewhat difficult to address. Thus, we will follow the formulation similar to [33][5] and introduce additional degrees of freedom representing the pressure amplitude(s). At this point, we may directly make the trivial extension to two different acoustic media coupled to the lower and upper surfaces and collect the corresponding pressure amplitudes in one vector $\mathbf{p}_\mathrm{n}$. The eigenvectors are extended accordingly as

$$\boldsymbol{\phi} = \begin{bmatrix} \mathbf{u}_\mathrm{n} \\ \mathbf{p}_\mathrm{n} \end{bmatrix}. \tag{18}$$

---

[5] In [33], the fluid was described in terms of the velocity potential rather than the pressure, and the discretization of the plate was achieved using spectral collocation rather than finite elements. However, these differences are of little relevance for the current discussion and the solution procedure proposed in this paper.
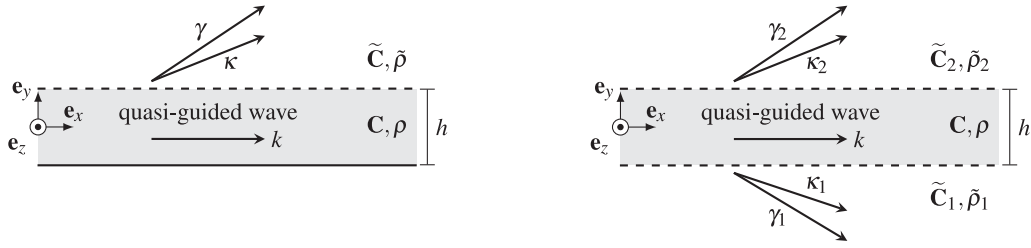
Fig. 3. Plate in contact with solid half-spaces at one or both of its surfaces.

In this approach, the coupling conditions are incorporated into the nonlinear eigenvalue problem (8), extending the involved matrices to account for the additional DOFs. The additional matrix entries due to the coupling can be read off from Eqs. (14) and (16). In particular, Eq. (14) introduces a term independent of k and ω and is thus to be included in the matrix $\overline{\mathbf{E}}_2$. Similarly, Eq. (16) involves a term proportional to ω^2 and can be incorporated into $\overline{\mathbf{M}}$. Finally, the left-hand side of (16) gives rise to terms in $\sqrt{\kappa^2 - k^2}$, which are included in a matrix of the form

$$\mathbf{R}(k) = \mathrm{i}\kappa_{y,1}\,\mathbf{R}_1 + \mathrm{i}\kappa_{y,2}\,\mathbf{R}_2, \tag{19}$$

with

$$\kappa_{y,1} = \sqrt{\kappa_1^2 - k^2}, \quad \kappa_{y,2} = \sqrt{\kappa_2^2 - k^2}. \tag{20}$$

Here, the indices 1,2 refer to the fluids coupled to the lower and upper surface. Specifically, if we denote by s_j the index of the DOF corresponding to the vertical displacement at interface $j = 1, 2$ and by f_j the index of the pressure-DOF, the matrix entries corresponding to coupling are

$$\overline{\mathbf{E}}_2^{s_j, f_j} = \pm 1, \qquad \overline{\mathbf{M}}^{f_j, s_j} = \pm\tilde{\rho}, \qquad \mathbf{R}_j^{f_j, f_j} = 1. \tag{21}$$

Overall, this means that we consider (16) to be an additional equation incorporated into $\overline{\mathbf{M}}$ and $\mathbf{R}_j$, while (14) is included in $\overline{\mathbf{E}}_2$ and represents the Neumann boundary condition imposed on the plate.

Remark 4. We may stress again that, in the case of $\kappa_1 = \kappa_2$ (i.e., a plate in contact with the same fluid medium at the lower and upper surface), the resulting eigenvalue problem can be linearized as discussed in [33]. While we will study such an example in our numerical experiments to verify the implementation, the main objective of the approach presented here is to address more complex problems, particularly those involving coupling to solid media or different materials (elastic or acoustic) at both surfaces.

4. Elastic plate embedded in an elastic medium

We now consider the situation in which the elastic plate is in contact with an elastic half-space or embedded in an elastic medium. For the beginning, let us again assume the presence of only one half-space coupled to the plate at $y = y_s$; see Fig. 3. The extension to two half-spaces of potentially different materials coupled to the lower and upper surfaces is straightforward. The fundamental solution of waves propagating in an isotropic horizontally stratified medium (assuming plane strain) can be found in the literature [58,59] and is only briefly reproduced here to fix notation. Again, we consider the waveguide to be aligned with the x-axis; thus, the wavenumber k of the guided wave modes matches the x-component of the wave vector in the surrounding medium. The displacements in the unbounded solid are a superposition of three plane waves, namely one longitudinal and two transverse waves. The latter are denoted as shear-vertical and shear-horizontal waves, respectively. The wavenumbers of longitudinal and transverse waves are denoted as κ and γ, and the respective vertical components of the wave vector are

$$\kappa_y = \pm\sqrt{\kappa^2 - k^2}, \qquad \gamma_y = \pm\sqrt{\gamma^2 - k^2}, \tag{22}$$

leading to nonlinearities similar to the case of fluid loading discussed before. Accounting for these observations, we write the displacements $\overline{\mathbf{u}} = \bar{u}_i \mathbf{e}_i$ in the unbounded solid as

$$\overline{\mathbf{u}}(x, y, t) = \nabla\varphi + \nabla \times \boldsymbol{\psi} + \partial_x \chi, \qquad y \notin \mathcal{I}, \tag{23}$$

where φ is the scalar potential of the longitudinal wave, $\boldsymbol{\psi}$ represents the vector potential of the shear-vertical wave, and χ describes the shear-horizontal wave. The potentials are assumed as

$$\varphi = a\,\mathrm{e}^{\mathrm{i}(kx + \kappa_y y - \omega t)}, \tag{24a}$$

$$\boldsymbol{\psi} = b\,\mathbf{e}_z\,\mathrm{e}^{\mathrm{i}(kx + \gamma_y y - \omega t)}, \tag{24b}$$

$$\chi = c\,\mathbf{e}_z\,\mathrm{e}^{\mathrm{i}(kx + \gamma_y y - \omega t)} \tag{24c}$$

with unknown wave amplitudes a, b, c. Substituting Eqs. (24) into (23) yields

$$\overline{\mathbf{u}}(x, y, t) = \left[(\mathrm{i}k\,\mathbf{e}_x + \mathrm{i}\kappa_y\,\mathbf{e}_y)\,a\,\mathrm{e}^{\mathrm{i}\kappa_y y} + (\mathrm{i}\gamma_y\,\mathbf{e}_x - \mathrm{i}k\,\mathbf{e}_y)\,b\,\mathrm{e}^{\mathrm{i}\gamma_y y} + \mathrm{i}k\,\mathbf{e}_z\,c\,\mathrm{e}^{\mathrm{i}\gamma_y y} \right] \mathrm{e}^{\mathrm{i}(kx-\omega t)}, \tag{25}$$

which we may write compactly as

$$\overline{\mathbf{u}}(x, y, t) = \mathbf{A}(k)\,\mathrm{e}^{\mathrm{i}\mathbf{D}y}\,\mathrm{e}^{\mathrm{i}(kx-\omega t)}\,\mathbf{c} \tag{26}$$

with

$$\mathbf{A}(k) = \begin{bmatrix} \mathrm{i}k & \mathrm{i}\gamma_y & 0 \\ \mathrm{i}\kappa_y & -\mathrm{i}k & 0 \\ 0 & 0 & \mathrm{i}k \end{bmatrix}, \tag{27}$$

$$\mathbf{D} = \mathrm{diag}[\kappa_y, \gamma_y, \gamma_y], \qquad \mathbf{c} = (a, b, c)^{\mathrm{T}}. \tag{28}$$

Compared to the formulation used for describing a surrounding fluid, we have now introduced the unknowns $\mathbf{c}$ rather than the acoustic pressure. We will also require the amplitudes of tractions acting on a plane parallel to the x-z-plane, cf. Section 2.1:

$$\overline{\boldsymbol{\tau}}(x, y) = \widetilde{\mathbf{C}}_{yx}\,\partial_x\overline{\mathbf{u}}(x, y) + \widetilde{\mathbf{C}}_{yy}\,\partial_y\overline{\mathbf{u}}(x, y). \tag{29}$$

Substituting Eqs. (26) into (29) yields

$$\overline{\boldsymbol{\tau}}(x, y) = \mathrm{i}k\,\widetilde{\mathbf{C}}_{yx}\,\mathbf{A}\,\mathrm{e}^{\mathrm{i}\mathbf{D}y}\,\mathrm{e}^{\mathrm{i}(kx-\omega t)}\mathbf{c} + \mathrm{i}\widetilde{\mathbf{C}}_{yy}\,\mathbf{A}\,\mathbf{D}\,\mathrm{e}^{\mathrm{i}\mathbf{D}y}\,\mathrm{e}^{\mathrm{i}(kx-\omega t)}\mathbf{c}. \tag{30}$$

To define the coupling conditions, we evaluate the displacement amplitudes at the interface $y = y_s$ based on Eq. (26). Recalling that $\overline{\mathbf{u}}(x, y, t) = \mathbf{u}(k, y, \omega)\,\mathrm{e}^{\mathrm{i}(kx-\omega t)}$, we obtain

$$\mathbf{u}(y = y_s) = \mathbf{A}\,\mathbf{c}_s \tag{31}$$

with

$$\mathbf{c}_s = \mathrm{e}^{\mathrm{i}\mathbf{D}y_s}\,\mathbf{c}. \tag{32}$$

Eq. (31) is expanded as

$$\mathbf{u}(y = y_s) = (\mathrm{i}k\mathbf{A}_0 + \mathrm{i}\kappa_y\mathbf{A}_1 + \mathrm{i}\gamma_y\mathbf{A}_2)\mathbf{c}_s \tag{33}$$

with

$$\mathbf{A}_0 = \begin{bmatrix} 1 & 0 & 0 \\ 0 & -1 & 0 \\ 0 & 0 & 1 \end{bmatrix}, \qquad \mathbf{A}_1 = \begin{bmatrix} 0 & 0 & 0 \\ 1 & 0 & 0 \\ 0 & 0 & 0 \end{bmatrix}, \qquad \mathbf{A}_2 = \begin{bmatrix} 0 & 1 & 0 \\ 0 & 0 & 0 \\ 0 & 0 & 0 \end{bmatrix}. \tag{34}$$

The second coupling condition is obtained by evaluating the traction amplitudes at the interface. This results in

$$\begin{aligned} \boldsymbol{\tau}(y = y_s) &= \mathrm{i}k\,\widetilde{\mathbf{C}}_{yx}\,\mathbf{A}\,\mathbf{c}_s + \mathrm{i}\widetilde{\mathbf{C}}_{yy}\,\mathbf{A}\,\mathbf{D}\,\mathbf{c}_s \\ &= -k\widetilde{\mathbf{C}}_{yx}\,(k\mathbf{A}_0 + \kappa_y\mathbf{A}_1 + \gamma_y\mathbf{A}_2)\,\mathbf{c}_s - \widetilde{\mathbf{C}}_{yy}\,(k\mathbf{A}_0 + \kappa_y\mathbf{A}_1 + \gamma_y\mathbf{A}_2)\,\mathbf{D}\,\mathbf{c}_s, \end{aligned} \tag{35}$$

where we have used again (33). We further introduce

$$\mathbf{D}_1 = \mathrm{diag}[1, 0, 0], \quad \mathbf{D}_2 = \mathrm{diag}[0, 1, 1] \tag{36}$$

such that $\mathbf{D} = \kappa_y\mathbf{D}_1 + \gamma_y\mathbf{D}_2$ and note that

$$\mathbf{A}_1\,\mathbf{D}_2 = \mathbf{A}_2\,\mathbf{D}_1 = 0, \quad \mathbf{A}_1\,\mathbf{D}_1 = \mathbf{A}_1, \quad \mathbf{A}_2\,\mathbf{D}_2 = \mathbf{A}_2, \quad \mathbf{A}_0\,\mathbf{D}_1 = \mathbf{D}_1, \quad \mathbf{A}_0\,\mathbf{D}_2 = -\mathbf{D}_2. \tag{37}$$

Hence, the above expression for the traction is simplified as

$$\boldsymbol{\tau}(y = y_s) = (k^2\mathbf{T}_0 + k\kappa_y\,\mathbf{T}_1 + k\gamma_y\,\mathbf{T}_2 + \kappa^2\mathbf{T}_3 + \gamma^2\mathbf{T}_4)\,\mathbf{c}_s \tag{38}$$

with

$$\mathbf{T}_0 = -(\widetilde{\mathbf{C}}_{yx}\mathbf{A}_0 - \widetilde{\mathbf{C}}_{yy}\mathbf{A}_1 - \widetilde{\mathbf{C}}_{yy}\mathbf{A}_2), \tag{39a}$$

$$\mathbf{T}_1 = -(\widetilde{\mathbf{C}}_{yx}\mathbf{A}_1 + \widetilde{\mathbf{C}}_{yy}\mathbf{D}_1), \tag{39b}$$

$$\mathbf{T}_2 = -(\widetilde{\mathbf{C}}_{yx}\mathbf{A}_2 - \widetilde{\mathbf{C}}_{yy}\mathbf{D}_2), \tag{39c}$$

$$\mathbf{T}_3 = -\widetilde{\mathbf{C}}_{yy}\mathbf{A}_1, \tag{39d}$$

$$\mathbf{T}_4 = -\widetilde{\mathbf{C}}_{yy}\mathbf{A}_2. \tag{39e}$$

To describe the plate coupled to an infinite solid medium, we introduce the conditions defined by Eqs. (33) and (38) (for two different media at the two surfaces if necessary) into the nonlinear eigenvalue problem. To this end, we multiply Eq. (33) by $\mathrm{i}k$; hence, all

coupling terms are either proportional to $k\kappa_y$ or $k\gamma_y$ or can be integrated into the existing matrices $\overline{\mathbf{E}}_0$, $\overline{\mathbf{E}}_1$, $\overline{\mathbf{E}}_2$. The eigenvector contains the nodal displacements $\mathbf{u}_n$ in the plate and the plane wave amplitudes in the unbounded media, which we abbreviate as $\mathbf{c}_n$:

$$\boldsymbol{\phi} = \begin{bmatrix} \mathbf{u}_n \\ \mathbf{c}_n \end{bmatrix}. \tag{40}$$

Analogously to Eq. (19), we introduce terms describing the interaction with the unbounded media. In the general case of two half-spaces consisting of different materials, the additional matrix function in the nonlinear eigenvalue problem is of the form

$$\mathbf{R}(k) = k\kappa_{y,1}\,\mathbf{R}_{1,1} + k\gamma_{y,1}\,\mathbf{R}_{2,1} + k\kappa_{y,2}\,\mathbf{R}_{1,2} + k\gamma_{y,2}\,\mathbf{R}_{2,2}. \tag{41}$$

The additional terms to be included in the matrices $\overline{\mathbf{E}}_0$, $\overline{\mathbf{E}}_1$, $\overline{\mathbf{E}}_2$ are directly given by Eqs. (33) and (38). Denoting by p_j and q_j the DOFs corresponding to the plate and unbounded domain at interface j, respectively, the components introduced by the coupling conditions are

$$\overline{\mathbf{E}}_0^{p_j,q_j} = \mp\mathbf{T}_{0,j}, \qquad \mathbf{R}_{1,j}^{p_j,q_j} = \pm\mathbf{T}_{1,j}, \qquad \mathbf{R}_{2,j}^{p_j,q_j} = \pm\mathbf{T}_{2,j}, \qquad \overline{\mathbf{E}}_2^{p_j,q_j} = \mp\kappa_j^2\,\mathbf{T}_{3,j} \mp \gamma_j^2\,\mathbf{T}_{4,j},$$

$$\overline{\mathbf{E}}_1^{q_j,p_j} = -\mathbf{I}, \qquad \overline{\mathbf{E}}_0^{q_j,q_j} = \mathbf{A}_0, \qquad \mathbf{R}_{1,j}^{q_j,q_j} = -\mathbf{A}_1, \qquad \mathbf{R}_{2,j}^{q_j,q_j} = -\mathbf{A}_2. \tag{42}$$

5. Solution procedure

5.1. Solving the NLEVP

This section summarizes the approach we employ for solving the nonlinear eigenvalue problems derived before. The key is to realize that, in the particular cases encountered here, we can rewrite the NLEVP as a linear multiparameter eigenvalue problem. In particular, this is achieved by generalizing the transformation in [43, Lemma 2.5], which relies on introducing auxiliary variables. For the so-obtained multiparameter eigenvalue problem, established algorithms exist, and their implementation is publicly available [48]. Hence, we will not delve into the numerical details of the computation. For the sake of tangibility, we present, in this section, a rather general and clear form of the multiparameter eigenvalue problem, albeit it is not always the most efficient version. Some comments and suggestions for improving efficiency are given in the appendix. The following theorem illustrates how the problem can be cast into a multiparameter eigenvalue problem.

Theorem 1. *If $(k, \boldsymbol{\phi})$ is a solution to* (8) *with $\mathbf{R}(k)$ given by* (19), *then the parameters ik, $i\kappa_{y,1}$, $i\kappa_{y,2}$, ξ_0 form a solution to the four-parameter eigenvalue problem*

$$\left(-\overline{\mathbf{E}}_2 + \omega^2\,\overline{\mathbf{M}} + ik\,\overline{\mathbf{E}}_1 + i\kappa_{y,1}\mathbf{R}_1 + i\kappa_{y,2}\mathbf{R}_2 + \xi_0\,\overline{\mathbf{E}}_0 \right)\boldsymbol{\phi} = \mathbf{0} \tag{43a}$$

$$\left(\begin{bmatrix} 0 & -\kappa_1^2 \\ 1 & 0 \end{bmatrix} + i\kappa_{y,1}\begin{bmatrix} 1 & 0 \\ 0 & 1 \end{bmatrix} + \xi_0\begin{bmatrix} 0 & -1 \\ 0 & 0 \end{bmatrix} \right)\mathbf{x}_1 = \mathbf{0} \tag{43b}$$

$$\left(\begin{bmatrix} 0 & -\kappa_2^2 \\ 1 & 0 \end{bmatrix} + i\kappa_{y,2}\begin{bmatrix} 1 & 0 \\ 0 & 1 \end{bmatrix} + \xi_0\begin{bmatrix} 0 & -1 \\ 0 & 0 \end{bmatrix} \right)\mathbf{x}_2 = \mathbf{0} \tag{43c}$$

$$\left(\begin{bmatrix} 0 & 0 \\ 0 & 1 \end{bmatrix} + ik\begin{bmatrix} 0 & 1 \\ 1 & 0 \end{bmatrix} + \xi_0\begin{bmatrix} 1 & 0 \\ 0 & 0 \end{bmatrix} \right)\mathbf{x}_3 = \mathbf{0} \tag{43d}$$

where

$$\kappa_{y,1}^2 := \kappa_1^2 - k^2, \quad \kappa_{y,2}^2 := \kappa_2^2 - k^2, \quad \xi_0 = -k^2 \tag{44}$$

and $\mathbf{x}_1 \neq 0$, $\mathbf{x}_2 \neq 0$ and $\mathbf{x}_3 \neq 0$.

Proof. The first Eq. (43a) is satisfied by the definition of $\kappa_{y,1}$, $\kappa_{y,2}$ and ξ_0 in (44). The determinant of the matrix in (43b) is $\kappa_1^2 + \xi_0 - \kappa_{y,1}^2$, which vanishes for $\kappa_{y,1}$ and ξ_0 given in the definition (44). Since the matrix is singular, there exists a non-zero vector $\mathbf{x}_1$ such that (43b) is satisfied. Eq. (43c) follows analogously. The determinant of the matrix in (43d) is $\xi_0 + k^2$, which is zero for the definition of ξ_0, and there exists a non-zero vector $\mathbf{x}_3$ such that (43d) is satisfied. $\square$

The above construction is by no means unique, i.e., there are other ways to build a multiparameter eigenvalue problem containing the solutions of the original problem. However, it is the formulation with the smallest number of additional auxiliary variables that we could find for the general case. Moreover, we built it such that if all matrices of the original problem (finite-element matrices and coupling matrices) are real, then all matrices of the multiparameter eigenvalue problem (43) are real. This is important for numerical computations as it is well known that eigenvalue problems with real matrices can generally be solved faster than problems with complex matrices (irrespective of whether the eigenvalues are real-valued).

For special cases, there are transformations with fewer variables. In the case where the plate is either coupled to a fluid only at one of its surfaces or to the same fluid at both surfaces, we may simply eliminate one parameter, say $\kappa_{y,2}$, and remove the corresponding third equation in the above system, yielding a three-parameter eigenvalue problem. Specifically, in the case of the same fluid on both sides, we have $\kappa_{y,1} = \kappa_{y,2}$ and hence $\kappa_{y,1}\mathbf{R}_1 + \kappa_{y,2}\mathbf{R}_2 =: \kappa_{y_1}\mathbf{R}$. However, as mentioned before, there are more

efficient ways to solve this special case [33]. Another important special case is the one where the plate consists only of isotropic materials, in which case the problem can be further simplified as shown in Appendix D.

For coupling to solid media, $\mathbf{R}(k)$ is given by (41). In this case we introduce new parameters

$$\xi_1 = k\kappa_{y,1}, \quad \xi_2 = k\gamma_{y,1}, \quad \xi_3 = k\kappa_{y,2}, \quad \xi_4 = k\gamma_{y,2} \tag{45}$$

and, together with ik and ξ_0, obtain the six-parameter eigenvalue problem

$$\left(-\overline{\mathbf{E}}_2 + \omega^2\,\overline{\mathbf{M}} + ik\overline{\mathbf{E}}_1 + \xi_1\mathbf{R}_{1,1} + \xi_2\mathbf{R}_{2,1} + \xi_3\mathbf{R}_{1,2} + \xi_4\mathbf{R}_{2,2} + \xi_0\overline{\mathbf{E}}_0\right)\boldsymbol{\phi} = \mathbf{0} \tag{46a}$$

$$\left(\begin{bmatrix} 0 & -\kappa_1^2 \\ 0 & 0 \end{bmatrix} + \xi_1\begin{bmatrix} 1 & 0 \\ 0 & 1 \end{bmatrix} + \xi_0\begin{bmatrix} 0 & -1 \\ 1 & 0 \end{bmatrix}\right)\mathbf{x}_1 = \mathbf{0} \tag{46b}$$

$$\left(\begin{bmatrix} 0 & -\gamma_1^2 \\ 0 & 0 \end{bmatrix} + \xi_2\begin{bmatrix} 1 & 0 \\ 0 & 1 \end{bmatrix} + \xi_0\begin{bmatrix} 0 & -1 \\ 1 & 0 \end{bmatrix}\right)\mathbf{x}_2 = \mathbf{0} \tag{46c}$$

$$\left(\begin{bmatrix} 0 & -\kappa_2^2 \\ 0 & 0 \end{bmatrix} + \xi_3\begin{bmatrix} 1 & 0 \\ 0 & 1 \end{bmatrix} + \xi_0\begin{bmatrix} 0 & -1 \\ 1 & 0 \end{bmatrix}\right)\mathbf{x}_3 = \mathbf{0} \tag{46d}$$

$$\left(\begin{bmatrix} 0 & -\gamma_2^2 \\ 0 & 0 \end{bmatrix} + \xi_4\begin{bmatrix} 1 & 0 \\ 0 & 1 \end{bmatrix} + \xi_0\begin{bmatrix} 0 & -1 \\ 1 & 0 \end{bmatrix}\right)\mathbf{x}_4 = \mathbf{0} \tag{46e}$$

$$\left(\begin{bmatrix} 0 & 0 \\ 0 & 1 \end{bmatrix} + ik\begin{bmatrix} 0 & 1 \\ 1 & 0 \end{bmatrix} + \xi_0\begin{bmatrix} 1 & 0 \\ 0 & 0 \end{bmatrix}\right)\mathbf{x}_5 = \mathbf{0} \tag{46f}$$

with the definitions given in Eq. (44) and, additionally,

$$\gamma_{y,1}^2 := \gamma_1^2 - k^2, \quad \gamma_{y,2}^2 := \gamma_2^2 - k^2. \tag{47}$$

Note that the determinant of the matrix in Eq. (46b) (analogously for (46c)–(46e)) is now $\xi_0(\kappa_1^2 + \xi_0 - \kappa_{y,1}^2)$, which again vanishes for $\kappa_{y,1}$ and ξ_0 given by (44), but also for $k = 0$ (rigid body modes). Eq. (46f) again poses the relationship $\xi_0 = -k^2$ (cf. (43d)). Furthermore, if the plate is coupled to the same material on both sides or one of the surfaces is free, we can reduce the number of parameters. In this case, we can remove ξ_3 and ξ_4 and the corresponding fourth and fifth equations, resulting in a four-parameter eigenvalue problem. We can also account for the situation where the plate is coupled to a fluid medium at one surface and a solid at the other. In this case, we include one parameter for the fluid, say ξ_1, as in Eq. (43) and two parameters, say ξ_3, ξ_4, in the form of (46), resulting in a five-parameter eigenvalue problem.

To numerically solve (43) and (46), we employ the Matlab implementations of numerical methods for multiparameter eigenvalue problems available in [48]. Thus, we will not explain the numerical computation in much detail. The mentioned numerical methods proceed by first decoupling the system of EVPs given by (43) and (46) in the eigenvalues. Accordingly, ik is an eigenvalue of a generalized eigenvalue problem $\mathbf{\Delta}_1\mathbf{v} = ik\mathbf{\Delta}_0\mathbf{v}$, where matrices $\mathbf{\Delta}_0$ and $\mathbf{\Delta}_1$ are the so-called operator determinants. These matrices are of size $n_\Delta \times n_\Delta$ with $n_\Delta = \prod_{i=1}^r n_i$, i.e., the product of the sizes of the matrices in each equation, cf., (2). Specifically, the operator determinants are of size $8n_1 \times 8n_1$ for (43) and $32n_1 \times 32n_1$ for (46), where $n_1 \times n_1$ is the size of the matrices in (43a) or (46a). Hence, the computational effort increases rapidly with the number of sought parameters. The details on the construction of $\mathbf{\Delta}_0$ and $\mathbf{\Delta}_1$ from the matrices in (43) and (46) are summarized in Appendix B, see also [16] or [45]. The corresponding operator determinant $\mathbf{\Delta}_0$ for the multiparameter eigenvalue problems (43) and (46) is singular. It is known that in such case we can find eigenvalues using a generalized staircase-type numerical algorithm from [47], whose Matlab implementation is available in [48] as well. In Appendix C, we present a workaround for the particular problems (43) and (46) that uses a shift to avoid additional steps necessary to deal with a singular $\mathbf{\Delta}_0$, resulting in a more efficient computation.

A few remarks on the above formulation are in order. We solve the multiparameter eigenvalue problem for a set of given frequencies; hence, the frequency ω is treated as a constant rather than an additional parameter. On the other hand, k^2 is identified as an additional parameter in the notation adopted here. Alternatively, we could linearize Eqs. (43) and (46a) in k with a companion linearization, which doubles the size of the corresponding matrices. This is usually done when solving the quadratic eigenvalue problem corresponding to the free plate (Section 2.1). Both variants lead to operator determinants of the same size. However, the first variant offers the advantage that it can be written in such a way that all matrices in the multiparameter eigenvalue problems are real (provided that the finite-element matrices are real), making the computation more efficient. In the case of coupling to fluid media, the parameters directly correspond to k, k^2, $\kappa_{y,1}$, $\kappa_{y,2}$, the last two being the vertical wavenumbers in the two fluids. In contrast, coupling to solid media results in additional parameters of the form $k\kappa_y$ and $k\gamma_y$. Also note that, since we obtain these vertical wavenumbers together with the eigenvalues k, we can directly evaluate the solution at any location inside the unbounded domains.

5.2. Postprocessing

It is important to note that the solution procedure allows both positive and negative signs of all wavenumbers, including those of partial waves in the half-spaces. Specifically, we obtain all valid solutions with either sign of each vertical wavenumber, cf., Eq. (22). This is a natural consequence of enforcing conditions on only the square of the vertical wavenumbers, specifically, Eqs. (44) and (47). This, in turn, implies that we do not only compute solutions characterized by waves propagating *away* from the plate inside

the unbounded media, but also *towards* it. For a given physical setup, the relevant modes are selected in a postprocessing step. For instance, one may choose those solutions where the vertical wavenumbers of all partial waves in the top (bottom) half-spaces have positive (negative) real parts; i.e., all wave vectors of partial waves point away from the plate surface. This particular selection will be deployed for the most part in the examples section, partly because these results can be verified using the commercial software *disperse* [60,61]. However, based on the modeled experiment or the user's interest, other criteria may be more feasible or relevant. In particular, it seems more meaningful to determine those modes that radiate energy into the unbounded media (away from the plate). This can be assessed by computing the Poynting vector **P** based on the solution inside the halfspaces and checking the sign of the vertical component. For the acoustic fluid, the time-averaged Poynting vector (at $x = 0$, $y = y_s$)[6] is given as

$$\hat{\mathbf{P}}^f = \tfrac{1}{2}\mathfrak{R}(\mathbf{v}^* p), \tag{48}$$

where the asterisk denotes the complex conjugate, $\mathfrak{R}$ is the real part, and the particle velocity is obtained as

$$\mathbf{v} = -\mathrm{i}\omega\,\mathbf{u}. \tag{49}$$

Note that we require, for this purpose, only the vertical component

$$\hat{P}_y^f = \tfrac{1}{2}\mathfrak{R}(v_y^* p), \tag{50}$$

which is particularly trivial to evaluate at the plate's surface coupled to the fluid, since both the pressure and the vertical displacement are components of the eigenvector (as vertical displacements are continuous across the interface, we may use the displacement of the plate rather than computing the displacement inside the fluid). However, it is easy to check that, in a fluid halfspace, the direction of the Poynting vector coincides with that of the wave vector. Hence, both criteria described above result in the identical subset of modes. The same does *not* hold for a solid halfspace. There, the time-averaged Poynting vector is given as

$$\hat{\mathbf{P}}^s = -\tfrac{1}{2}\mathfrak{R}(\mathbf{v}^* \cdot \boldsymbol{\sigma}). \tag{51}$$

Again, to determine which modes propagate energy away from the plate, we only need to evaluate the y-component of this vector, i.e.,

$$\hat{P}_y^s = -\tfrac{1}{2}\mathfrak{R}(\mathbf{v}^* \cdot \boldsymbol{\tau}), \tag{52}$$

which is also simple to compute at the interface, where the traction $\boldsymbol{\tau}$ is readily given by Eq. (38). Employing this criterion reveals that there is typically a rather large number of modes that propagate energy away from the plate, even though a wave vector corresponding to one of the partial waves points towards the plate. We will see a comparison of these two different criteria in Section 6.4. Other solutions that exhibit a power flux towards the plate should nevertheless not be considered spurious. It could be interesting to study them in the context of, e.g., air-coupled or immersed ultrasonic testing or seismic waves interacting with soil layers. Also let us remember that, for some solutions, the vertical component of the Poynting vector may vanish (trapped modes). Thus, when employing this criterion in a numerical method, we will have to specify a threshold in the computation of the power flux depending on whether or not we wish to filter out such trapped modes. Finally, when presenting results of dispersion curves computed in this manner, one typically omits modes with an attenuation above a somewhat arbitrary value. In our numerical examples, the modes that are not within the chosen range of plotted attenuation are also omitted from the phase velocity plots.

6. Numerical examples

In order to validate and illustrate the competitiveness of our approach, we present four numerical examples that involve plate structures of different materials coupled to acoustic and elastic half-spaces. Homogeneous elastic plates are discretized by a single finite element whose polynomial degree p_e is chosen according to the recommendation given in [63] as

$$p_e = \left\lceil \frac{a_0}{2} \right\rceil + 3, \qquad a_0 = \frac{h\,\omega_{\max}}{c_s}. \tag{53}$$

Here, a_0 is a dimensionless frequency, computed based on the shear wave velocity c_s, layer thickness h, and maximum frequency of interest $\omega_{\max}$. The symbol $\lceil\cdot\rceil$ denotes the ceiling function, i.e., the result is rounded up to the next integer. In [63], this choice of the element order was designed such that the approximation error of any of the propagating modes at the given frequency and material does not exceed 0.1%. When modeling plates consisting of several layers, the polynomial degree of each layer is chosen separately based on its local shear wave velocity and thickness. For each example, we plot the dispersion curves in terms of phase velocity and attenuation. In addition, we visualize the wave fields created by two selected modes at different frequencies in order to provide some physical insight into the wave propagation behavior. The relevant parameters of all materials used in the examples are summarized in Table 1. All computations have been performed using a Matlab implementation of the proposed approach, executed on a desktop computer using an 11th Gen Intel Core i9-11900K processor (3.50 GHz) and 16 GB RAM. A minimal implementation of the examples presented in the following is publicly available [49]. They are also included in the open source software SAMWISE [50], which allows applying this methodology to user-defined structures.

---

[6] Note that the magnitude of the Poynting vector depends on the spatial coordinates x and y due to the imaginary part of the wavenumbers k and κ_y [62]. However, as we are interested solely in the *direction* of the power flux, it shall suffice to arbitrarily evaluate the Poynting vector at any position.

Table 1

Overview of material parameters used in the numerical experiments.

	Density ρ	Wave speeds c_ℓ, c_t		Lamé parameters λ, μ	
Brass	8.40 g/cm³	4.40 km/s	2.20 km/s	81.312 GPa	40.656 GPa
Teflon	2.20 g/cm³	1.35 km/s	0.55 km/s	2.679 GPa	0.666 GPa
Titanium	4.46 g/cm³	6.06 km/s	3.23 km/s	70.726 GPa	46.531 GPa
Water	1.00 g/cm³	1.48 km/s			
Oil	0.87 g/cm³	1.74 km/s			
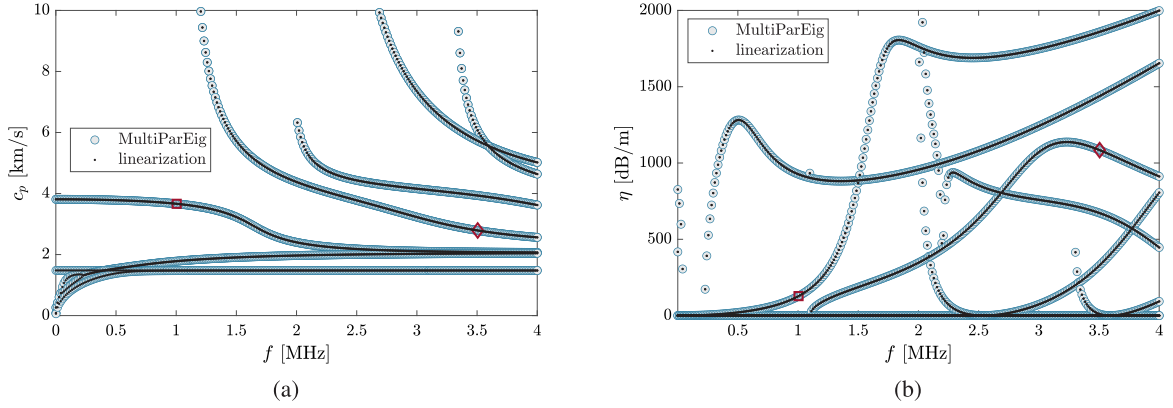
Fig. 4. (a) Phase velocity and (b) attenuation of guided waves in a 1 mm thick brass plate immersed in water. Results are computed using the proposed method ('MultiParEig') and validated against the alternative approach based on a linearization [33]. The symbols □ and ◇ indicate arbitrarily chosen modes whose wave fields are plotted in Fig. 7.

6.1. Brass plate immersed in water

As a first numerical experiment for validating the proposed approach, we consider waves propagating along a brass plate of thickness 1 mm immersed in water. We compute dispersion properties for 300 frequencies up to 4 MHz. According to Eq. (53) and considering the material parameters presented in Table 1, a discretization using one element with a polynomial degree of 9 (i.e., 10 nodes) is sufficient to obtain accurate results. We assume plane strain conditions, hence considering in-plane displacements only ('Lamb-type' modes). The shear-horizontal (out-of-plane) modes are omitted here as they do not couple to the acoustic medium. Consequently, we obtain finite-element matrices of size 22×22, including the two DOFs representing the pressure at the upper and lower surface. As the plate is coupled to the same fluid on both sides, we can employ, for validation, the simpler approach of linearizing the eigenvalue problem by means of a change of variables as described in [33]. In a postprocessing step, we select the modes that propagate away from the plate inside the halfspaces, see Section 5.2. Fig. 4 shows the dispersion curves in terms of phase velocity and attenuation. The approach proposed in this paper is labeled 'MultiParEig' (multiparameter eigenvalue problem), while 'linearization' refers to the method in [33]. Results are in excellent agreement with relative differences between eigenvalues below 0.1% when comparing both approaches. The computing time required for obtaining the complete dispersion curves was about 1.6 s (i.e., 5 ms per frequency) when exploiting the linearization described in Appendix D and 3.6 s without this improvement.

A particular challenge in modeling embedded waveguides is the occurrence of so-called trapped modes, which can be encountered when the horizontal wavenumber of a guided mode is larger than the free-field wavenumber in the adjacent unbounded medium. Such modes are characterized by a vanishing power flux through the waveguide's boundaries; hence, they propagate along the structure without attenuation, i.e., $\Im(k) = 0$. Moreover, the wave field of these modes is confined to the proximity of the waveguide, exhibiting an exponential decrease with the distance from the waveguide, $\Im(\kappa_y) > 0$. We show in Fig. 5 magnified parts of the dispersion curves together with the vertical component κ_y of the wavenumber in the fluid above the plate to demonstrate that the proposed approach is capable of representing correctly the behavior of the trapped modes as well as the known bifurcation of the A_0 mode. For detailed discussions on the behavior of these modes and their interpretation, the reader is referred to [34,56].

To better clarify the effect of the precise interface conditions, we present in Fig. 6, a comparison between the current approach and the approximate linear ('dashpot') boundary condition as described in [30,31]. While the dashpot approximation gives reasonably good results for the higher modes, it does not accurately represent the attenuation of modes with a phase velocity close to the wave speed in the fluid. In particular, it cannot accurately describe the trapped modes discussed above. This observation is in agreement with the discussion in [32], where it was concluded that the dashpot condition is a suitable technique in situations with a large acoustic mismatch at the interface and for relatively high frequencies. On the other hand, the dashpot boundary condition does not evoke significant computational costs compared to the free waveguide problem and is trivial to extend to arbitrary geometries [31]. In this particular example, the computing time required to obtain the dispersion curves was only about 0.1 s when using the dashpot boundary condition.
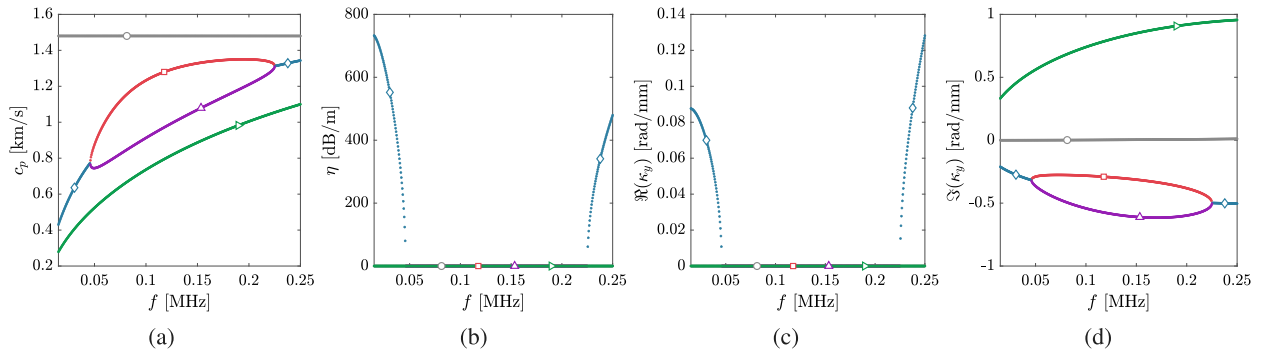
(a)   (b)   (c)   (d)

Fig. 5. (a,b) Details of the dispersion curves presented in Fig. 4 at small frequencies, together with the (c) real part and (d) imaginary part of the vertical wavenumber in the fluid. Note that $\Im(\kappa_y) \neq 0$ holds for all depicted modes, though the mode indicated by ⊸ takes very small positive values at the low frequencies shown here.
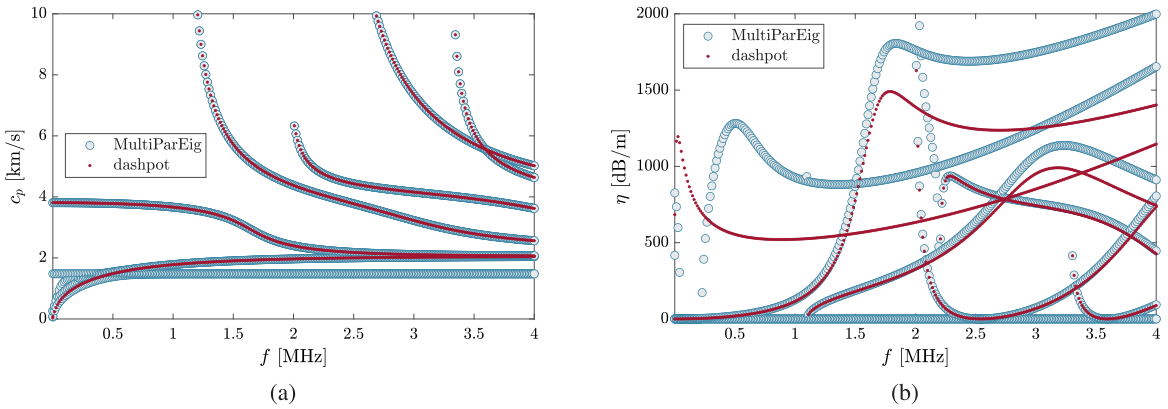

(a)   (b)

Fig. 6. Dispersion curves of the immersed brass plate, comparing the current approach ('MultiParEig') to the linear approximation ('dashpot') described in [30]. The dashpot approximation underestimates the attenuation due to radiation.

(a)   (b)
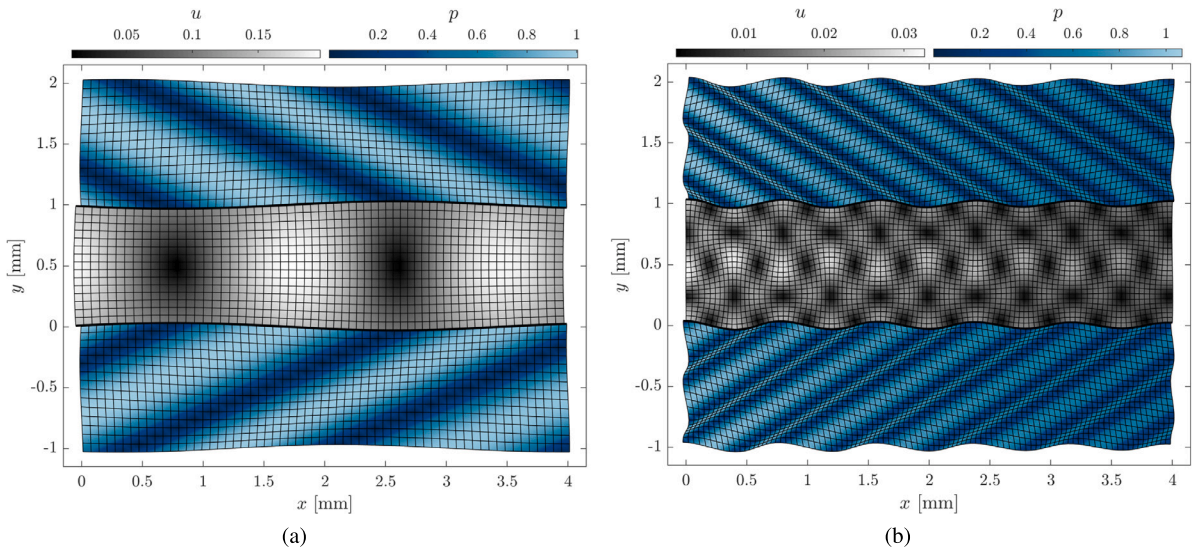
Fig. 7. Wave fields of two modes in the water-immersed brass plate at (a) 1 MHz and (b) 3.5 MHz. The modes are indicated in the dispersion diagram in Fig. 4 by the symbols □ and ◇.
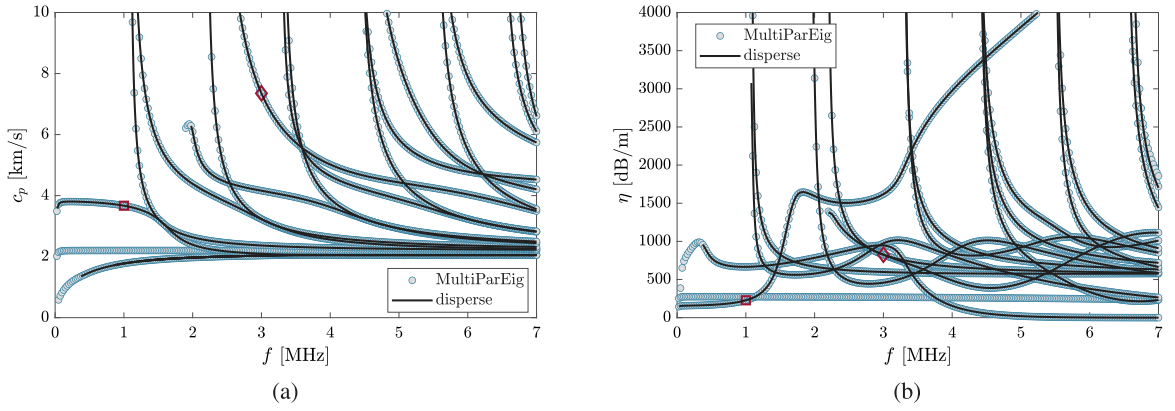
Fig. 8. (a) Phase velocity and (b) attenuation of guided waves in a 1 mm thick brass plate coupled on one side to infinite Teflon. Results are computed using the proposed FEM-based approach and validated against the software *disperse*.
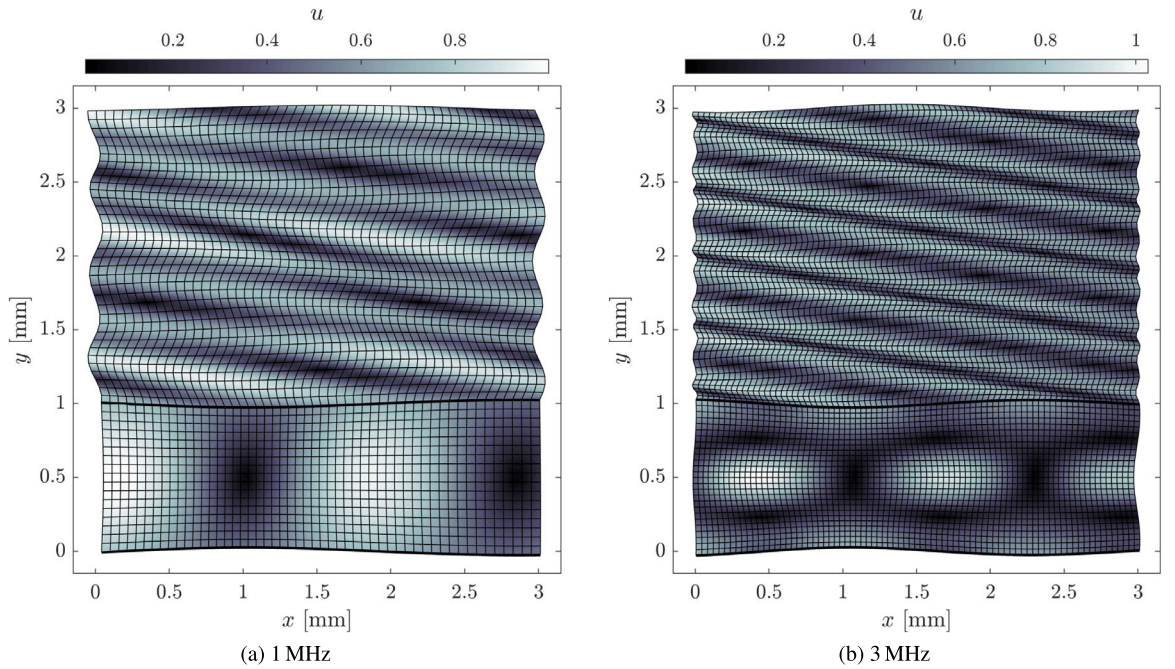

(a) 1 MHz

(b) 3 MHz

Fig. 9. Mode shapes in a brass plate coupled to Teflon of (a) the fundamental symmetric mode at 1 MHz and (b) the seventh propagating mode at 3 MHz. The modes are indicated in the dispersion diagram in Fig. 8 by the symbols □ and ◊.

In Fig. 7, we present the wave fields of two arbitrarily selected modes at 1 MHz and 3.5 MHz, indicated on the dispersion graphs in Fig. 4 as □ and ◊. The color scales represent the local magnitudes of acoustic pressure in the fluid and displacement in the plate, respectively. Note that, even though we only discretize the plate's thickness, the wave field anywhere inside the plate as well as in the surrounding medium can be evaluated in a post-processing step. In particular, the displacements inside the plate for arbitrary values of x are obtained by Eq. (4) and interpolation along the thickness using the finite-element trial functions. Similarly, the acoustic pressure in the water is evaluated based on Eq. (10), where the vertical wavenumbers have been obtained as solutions to the multiparameter eigenvalue problem. Furthermore, the particle displacement in the acoustic domains is obtained as

$$\mathbf{u}_p = \frac{1}{\omega^2 \rho} \nabla p, \tag{54}$$

which is visualized by the grid distortion in Fig. 7. As expected, it can be observed that the horizontal wavenumber in the acoustic domains matches that of the guided wave inside the plate. The horizontal displacement is discontinuous at the material interfaces since the fluid does not support shearing. At the higher frequency where the wavelength is small and attenuation due to energy leakage is significant (Fig. 7(b)), we can also note how the magnitude decreases as the wave propagates in positive x-direction.
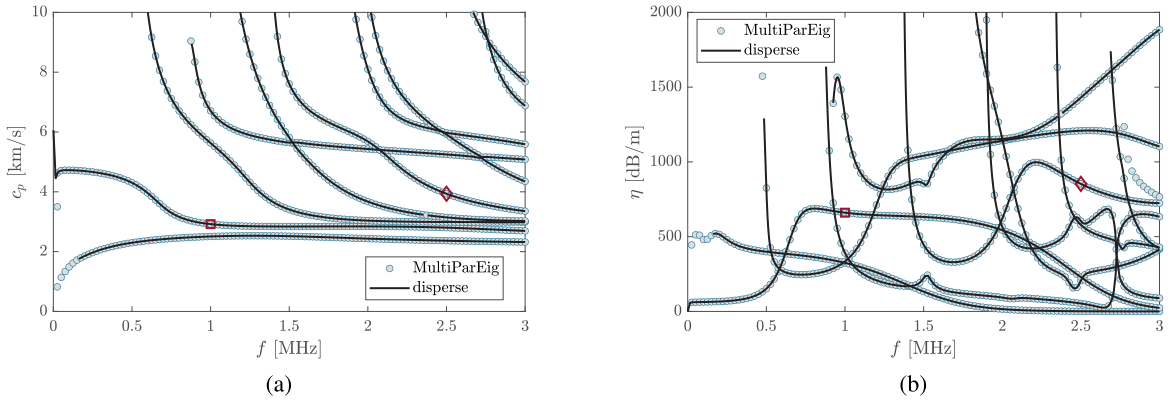
Fig. 10. (a) Phase velocity and (b) attenuation of guided wave modes in a layered plate (titanium-brass-titanium) between an elastic (Teflon) and a fluid (oil) half-space. Results are computed using the proposed FEM-based approach and validated against the software *disperse*.

6.2. Brass plate coupled to infinite Teflon

To validate the computation of waveguide modes radiating into another elastic medium, we consider the same 1 mm thick brass plate as in the previous example, now attached on one surface to a half-space with the elastic parameters of Teflon, as given in Table 1. The choice of this rather arbitrary example is motivated by the circumstance that it can be verified using the free demonstration version of the commercial software *disperse* [60,61]. Here, we compute dispersion curves up to a frequency of 7 MHz in increments of 25 kHz; hence, we require a finite element of order 13. In this example, we include not only the in-plane ('Lamb-modes'), but also the shear-horizontal modes that cause displacements in the out-of-plane direction z only. Consequently, we obtain matrices of size 45×45, including three DOFs for the unbounded domain. Phase velocity and attenuation of all leaky modes are shown in Fig. 8. The results are in excellent agreement between the proposed approach and the Global Matrix Method implemented in the *disperse* software. We obtained a few additional solutions where the automatic tracing algorithm in *disperse* failed to find the roots; apart from that, there is no discernible difference between the methods. For the purpose of this validation, we chose to plot only those modes with $\kappa_{y,1} \geq 0$ and $\gamma_{y,1} \geq 0$. Employing the criterion based on the direction of the power flux as mentioned in Section 5.2 yields additional solutions that are not included in those computed by *disperse*. The computational costs for this example are significantly larger compared to the simpler case in the previous subsection due to the larger number of parameters and larger matrix sizes, requiring about 35 s to compute the shown dispersion curves (123 ms per frequency). Again, we visualize in Fig. 9 the mode shapes of two modes at frequencies of 1 MHz and 3.5 MHz by computing the displacement field in a section of the plate and part of the adjacent medium. Since both materials are now elastic, both longitudinal and shear components are transmitted from the plate into the unbounded medium, and consequently, all displacement components are continuous at the interface.

6.3. Layered plate between a fluid and an elastic half-space

In this rather general example, we consider a multi-layered plate coupled to an elastic and a fluid half-space at the lower and upper surfaces, respectively. The plate itself consists of three layers (titanium-brass-titanium), each with a thickness of 1 mm. For the half-spaces, material parameters of Teflon and oil are assumed, as given in Table 1. For the brass layer, we require an element order of eight, while an order of six is sufficient for the titanium layers up to a frequency of 3 MHz. Assuming again a plane strain state with two displacement components per node, we obtain finite-element matrices of size 45×45, including the three DOFs (two displacements and one pressure) describing the unbounded domains. Dispersion curves are given in Fig. 10, computed at 121 frequencies with an increment of 25 kHz. The computing time was about 56 s (460 ms per frequency). Again, results agree well with the reference solution obtained using *disperse*, though some challenges were encountered in the application of the Global Matrix Method when trying to trace all modes over the entire frequency range. Fig. 11 illustrates the relatively complex mode shapes inside the multi-layered specimen compared to the previous examples.

6.4. Solid layer between two elastic half-spaces

As a final numerical study, we address the computationally most demanding case in which the plate is coupled to two different solid media at the lower and upper surfaces, leading to the six-parameter eigenvalue problem in Eq. (46). The layer consists of titanium, while the elastic parameters of Teflon (below the plate) and brass (above the plate) are assumed for the half-spaces. We choose a frequency range up to 10 MHz, requiring a finite element of order 13 to discretize the plate. The frequency increment was selected as 50 kHz. Results for the 'Lamb-type' modes are presented in Fig. 12. Again, a comparison is made with the software *disperse*, Fig. 12(a) and (b) showing the modes with vertical wavenumbers pointing away from the plate in both halfspaces. This example is particularly challenging due to the relatively small acoustic mismatch between titanium and brass, resulting in significant
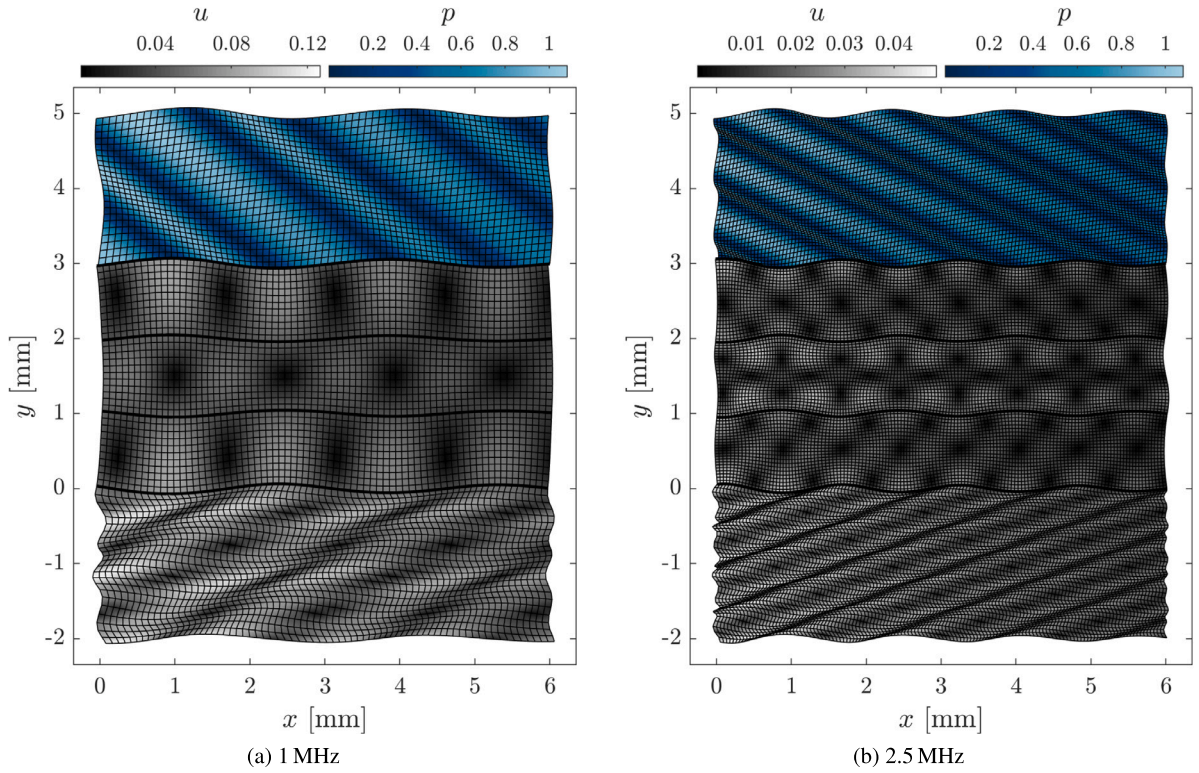
Fig. 11. Mode shapes of two waves at (a) 1 MHz and (b) 2.5 MHz for the trilayered plate (titanium-brass-titanium) between an elastic (Teflon) and a fluid (oil) half-space. The modes are indicated in the dispersion diagram in Fig. 12 by the symbols □ and ◇.

radiation into the upper half-space. When using *disperse*, – which requires tracing individual modes starting from isolated roots of the dispersion relation – finding all solutions is not straightforward. To achieve the shown comparison, we made extensive use of the software's feature to search for roots in regions where we expected to find modes based on our own computations. Still, we were not able to trace all branches over the entire frequency range in *disperse*, and for some modes, the tracing algorithm abruply switches to a different mode. To better illustrate this issue, we include in Fig. 12(c) and (d) all modes that do not propagate energy towards the plate (zoomed in for conciseness)[7]. This selection results in many additional modes compared to the criterion based on wavenumbers. These results clarify the difficulty of mode-tracing algorithms in the presence of many similar branches. It can also be noted that all roots found by *disperse* are among those valid solutions. The modes that were traced successfully agree well with our solutions, which shall suffice to demonstrate the validity of both formulations. Our approach required about 186 s to compute the dispersion curves (920 ms per frequency). The wave fields visualized in Fig. 13 help demonstrate the difficulty of this example. Due to the drastically different elastic constants between titanium and teflon, waves propagate with significantly smaller vertical wavelengths in the lower half-space. At the same time, the difference between titanium and brass is so small that the interface at $y = 1$ mm is hardly noticeable. However, even for this rather extreme case, the proposed approach yields robust results.

6.5. Accuracy and computational costs

The numerical examples demonstrate that the results obtained using the proposed approach are in excellent agreement with the Global Matrix Method implemented in *disperse* as well as with the linearization in the special case discussed in the first example. The formulation of the boundary conditions is exact and, hence, the coupling to unbounded domains does not give rise to inaccuracies apart from potential numerical errors in the solution of the multiparameter eigenvalue problem. The solution inside the layered structures, on the other hand, is approximated by finite elements and can be expected to converge to the exact solution in the usual manner when increasing the number of elements ('h-refinement') or the polynomial degree of the elements ('p-refinement'). We exemplarily demonstrate this behavior by means of the setup used in Section 6.3, as it involves coupling to both fluid and solid

---

[7] More specifically, we include modes with $\hat{P}_y^s > -0.01 \max(|\hat{P}_y^s|)$ at the top surface and $\hat{P}_y^s < 0.01 \max(|\hat{P}_y^s|)$ at the lower surface where $\max(|\hat{P}_y^s|)$ denotes the maximum vertical absolute power flux of all modes. This is to say, we include trapped modes with vanishing power flux through the plate surfaces.
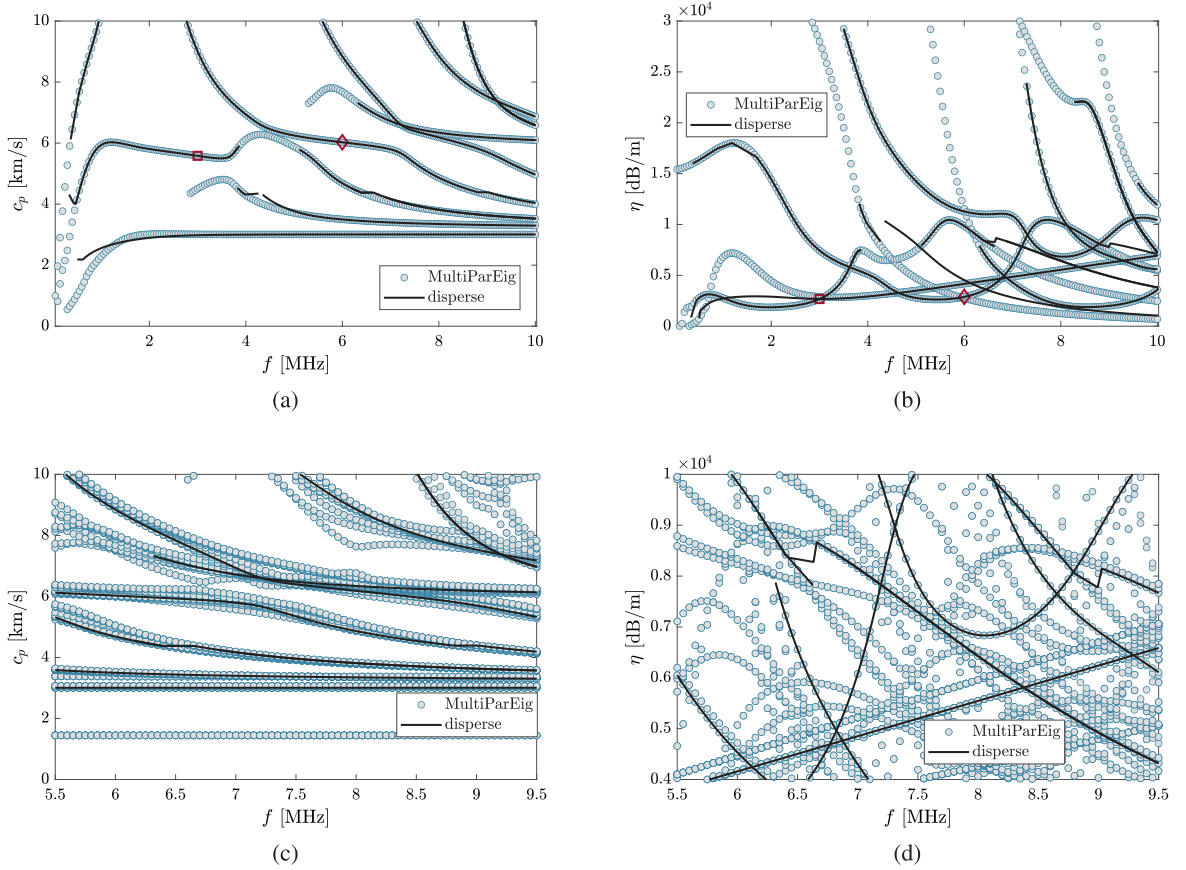
Fig. 12. Phase velocity and attenuation of guided wave modes in a 1 mm thick titanium plate between two elastic half-spaces consisting of brass and Teflon, respectively. Results are computed using the proposed FEM-based approach and validated against the software *disperse*. In (a) and (b), modes are selected based on the sign of the vertical wavenumber, while (c) and (d) result from employing the criterion based on the power flux.

media as well as a layered structure. Convergence is analyzed for the first eight modes at a frequency around 2 MHz (cf. Fig. 10). The error in eigenvalues is computed as

$$\epsilon = \sqrt{\frac{\sum_{i=1}^{8} |k_i - \bar{k}_i|^2}{\sum_{i=1}^{8} |\bar{k}_i|^2}}, \tag{55}$$

where $\bar{k}_i$ denote the reference solutions obtained using *disperse*. Fig. 14 shows the convergence of this error when increasing the size n_1 of the finite-element matrices. When using a constant element order p_e and increasing the number of elements (shown for element orders of $p_e = 1$ and $p_e = 2$), the error is expected to behave asymptotically as $n_1^{-2p_e}$ for sufficiently smooth problems, which is confirmed by the results. More precisely, the slopes computed between the last two points of these graphs equal 2.01 and 3.99, respectively. In addition, we show the convergence of the error when increasing the polynomial degree of the elements while keeping their number constant (here one element per layer). As has been discussed in detail in previous studies [63,64], this discretization scheme converges rapidly (exponentially under optimal conditions) and, hence, has been used to choose the finite element mesh as discussed in the beginning of this section. In Fig. 14, we also list the reference values used in this study as obtained from *disperse*.

As mentioned before, the computational costs for solving the multiparameter eigenvalue problem can become significant when increasing the size of the finite-element matrices n_1 or the number of parameters r. To illustrate this relationship more concisely, we plot in Fig. 15 the computing times used for solving the multiparameter eigenvalue problem at one frequency (here 1 MHz) for varying values of n_1 and r. To obtain these results, we have used the same examples described above, since they cover all cases from $r = 2$ to $r = 6$. The matrix size n_1 has been increased by varying the element order. We may note that in the case of $r = 2$ (coupling to one fluid), the computing time is still around 0.1 s when the matrix size exceeds 100×100. When considering the coupling to two different solid media ($r = 6$), the computing time is around 50 s for similar n_1. However, the numerical studies confirm that, in many typical scenarios, the size of the finite-element matrices can be kept well below $n_1 = 100$ as long as we make use of efficient high-order discretizations.
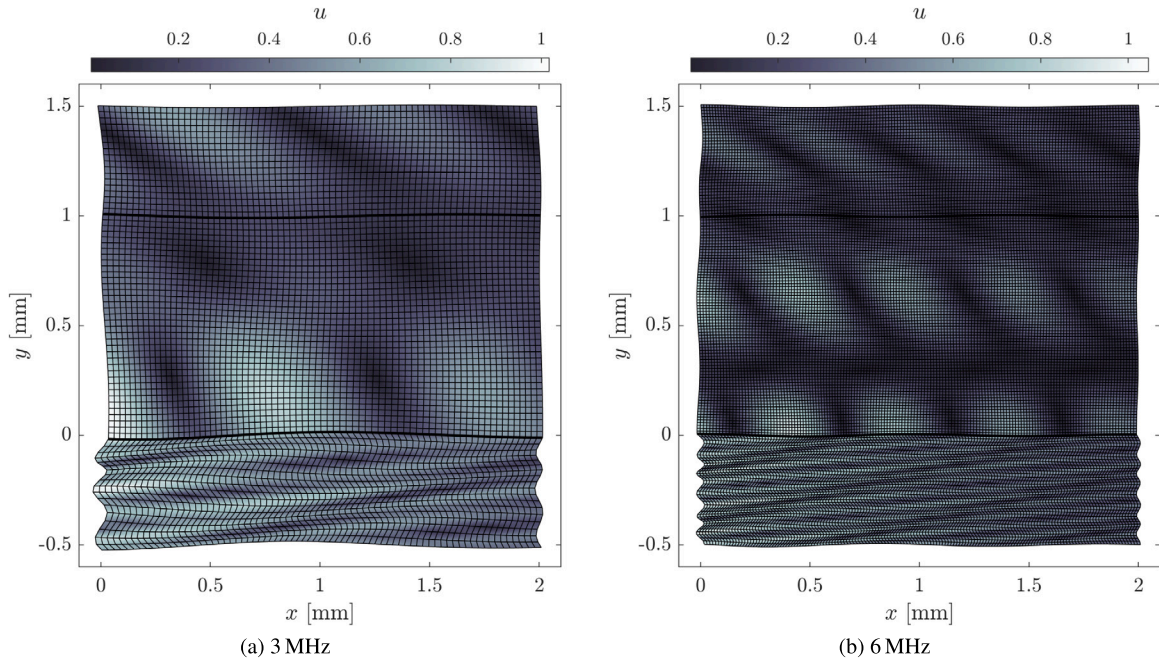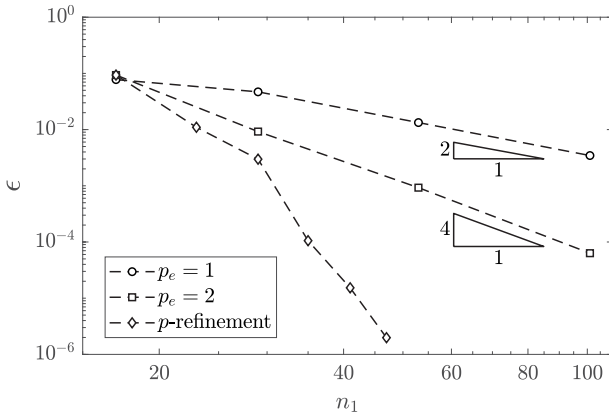
Fig. 13. Mode shapes of two modes at (a) 3 MHz and (b) 6 MHz for the titanium plate between a Teflon half-space (below) and a brass half-space (above). The modes are indicated in the dispersion diagram in Fig. 12 by the symbols □ and ◇.

| f [MHz]	c_p [km/s]	η [dB/m]
1.99590	2.43522	15.8025
2.01523	3.03322	1144.36
2.00532	3.66113	1154.06
2.01504	5.42525	90.5988
1.99678	5.69435	612.243
1.99882	8.11628	1160.14
2.08320	2.84053	509.200
1.96527	8.75104	1308.75
reference solution		

Fig. 14. Convergence of the error in eigenvalues when increasing the number of elements of a given polynomial degree ($p_e = 1$, $p_e = 2$) and for constant number of elements when increasing the polynomial degree (p-refinement). The table shows the reference solution used to compute the error.

7. Conclusions

We have demonstrated that the interface conditions arising from the coupling between an elastic layered medium and adjacent acoustic or elastic unbounded domains can be incorporated into a conventional semi-analytical waveguide model. The resulting nonlinear eigenvalue problem is solved by exploiting the connection to multiparameter eigenvalue problems, for which established algorithms are available. As a result, we obtain the wavenumbers of guided waves, as well as those in the adjacent media, together with the corresponding semi-discretized mode shapes. These problems are computationally relatively demanding to solve compared to those of free plates. This is particularly true in the case of two adjacent elastic media, which require the solution of generalized eigenvalue problems more than 32 times larger than that describing the free plate. Nevertheless, we demonstrated that the computational costs are manageable for relevant applications when using efficient discretization schemes to model the plate. As of now, we have restricted the presented formulation to isotropic and nondissipative half-spaces (while the plate's material can be anisotropic). This limitation may be possible to overcome by generalizations to be done in future work.
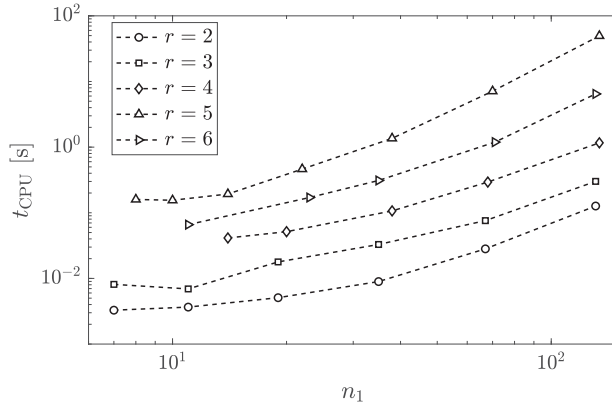
example	r	n_1	n_Δ	t_{CPU} [s]
6.1*	2	22	44	0.005
6.1	3	22	88	0.012
6.2	4	45	360	0.123
6.3	5	45	720	0.460
6.4	6	32	1024	0.920

* linearization according to Appendix D

Fig. 15. Computational time t_{CPU} used for solving the multiparameter eigenvalue problem for varying matrix size n_1 and number of parameters r. The table lists the matrix sizes and computational times per frequency for our numerical examples with the discretizations used in the respective sections.

CRediT authorship contribution statement

Hauke Gravenkamp: Writing – original draft, Visualization, Software, Methodology, Conceptualization. **Bor Plestenjak:** Writing – original draft, Software, Methodology, Conceptualization. **Daniel A. Kiefer:** Writing – review & editing, Software, Methodology, Conceptualization. **Elias Jarlebring:** Writing – review & editing, Supervision, Conceptualization.

Declaration of competing interest

The authors declare that they have no known competing financial interests or personal relationships that could have appeared to influence the work reported in this paper.

Data availability

No data was used for the research described in the article.

Acknowledgments

Appendix A. Finite-element matrices

Applying a finite-element discretization to the weak form (6) involves choosing an approximation of the displacement amplitudes

$$\mathbf{u} = \mathbf{N}(\zeta)\mathbf{u}_n, \tag{A.1}$$

where $\mathbf{u}_n$ is the vector of nodal values, and $\mathbf{N}$ is the matrix of shape functions defined in the element's local coordinate ζ. The FE matrices are obtained as [14,65]

$$\mathbf{E}_0 = \int_{-1}^{1} \mathbf{B}_1^T \hat{\mathbf{C}} \mathbf{B}_1 |J|\, d\zeta, \quad \mathbf{E}_1 = \int_{-1}^{1} \left(\mathbf{B}_1^T \hat{\mathbf{C}} \mathbf{B}_2 - \mathbf{B}_2^T \hat{\mathbf{C}} \mathbf{B}_1 \right) |J|\, d\zeta, \quad \mathbf{E}_2 = \int_{-1}^{1} \mathbf{B}_2^T \hat{\mathbf{C}} \mathbf{B}_2 |J|\, d\zeta, \quad \mathbf{M} = \rho \int_{-1}^{1} \mathbf{N}^T \mathbf{N} |J|\, d\zeta, \tag{A.2}$$

where $\hat{\mathbf{C}}$ denotes the elasticity matrix in Voigt notation, $|J|$ is the Jacobian defining the coordinate transformation from y to ζ, and $\mathbf{B}_1, \mathbf{B}_2$ are defined as

$$\mathbf{B}_1 = \mathbf{b}_1 \mathbf{N}, \qquad \mathbf{B}_2 = \frac{1}{y_{,\zeta}} \mathbf{b}_2 \mathbf{N}_{,\zeta}, \quad \text{with} \quad \mathbf{b}_1 = \begin{bmatrix} 0 & 0 & 1 \\ 0 & 1 & 0 \end{bmatrix}^T, \qquad \mathbf{b}_2 = \begin{bmatrix} 1 & 0 & 0 \\ 0 & 0 & 1 \end{bmatrix}^T. \tag{A.3}$$

18

Appendix B. Multiparameter eigenvalue problems and operator determinants

An *r-parameter eigenvalue problem* has the form

$$(\mathbf{A}_{i0} + \lambda_1 \mathbf{A}_{i1} + \cdots + \lambda_r \mathbf{A}_{ir}) \mathbf{x}_i = \mathbf{0}, \qquad i = 1, \ldots, r, \tag{B.1}$$

where $\mathbf{A}_{ij}$ is an $n_i \times n_i$ matrix and $\mathbf{x}_i \neq \mathbf{0}$ for $i = 1, \ldots, r$. If (B.1) is satisfied then the tuple $(\lambda_1, \ldots, \lambda_r)$ is an *eigenvalue* and $\mathbf{z} = \mathbf{x}_1 \otimes \cdots \otimes \mathbf{x}_r$ is the corresponding *eigenvector*, where "$\otimes$" denotes the Kronecker product.[8] The problem (B.1) is related to a system of r generalized eigenvalue problems

$$\boldsymbol{\Delta}_i \mathbf{z} = \lambda_i \boldsymbol{\Delta}_0 \mathbf{z}, \qquad i = 1, \ldots, r, \tag{B.2}$$

where the matrices

$$\boldsymbol{\Delta}_0 = \begin{vmatrix} \mathbf{A}_{11} & \cdots & \mathbf{A}_{1r} \\ \vdots & & \vdots \\ \mathbf{A}_{r1} & \cdots & \mathbf{A}_{rr} \end{vmatrix}_\otimes = \sum_{\sigma \in S_r} sgn(\sigma) \, \mathbf{A}_{1\sigma_1} \otimes \mathbf{A}_{2\sigma_2} \otimes \cdots \otimes \mathbf{A}_{r\sigma_r} \tag{B.3}$$

and

$$\boldsymbol{\Delta}_i = (-1) \begin{vmatrix} \mathbf{A}_{11} & \cdots & \mathbf{A}_{1,i-1} & \mathbf{A}_{10} & \mathbf{A}_{1,i+1} & \cdots & \mathbf{A}_{1r} \\ \vdots & & \vdots & \vdots & \vdots & & \vdots \\ \mathbf{A}_{r1} & \cdots & \mathbf{A}_{r,i-1} & \mathbf{A}_{r0} & \mathbf{A}_{r,i+1} & \cdots & \mathbf{A}_{rr} \end{vmatrix}_\otimes, \qquad i = 1, \ldots, r, \tag{B.4}$$

are called operator determinants. For details see, e.g., [66]. Note that (B.3) is a generalized Leibniz formula for the determinant, where we sum over all permutations σ in the permutation group S_r, with the Kronecker product instead of the usual product. If $\boldsymbol{\Delta}_0$ is nonsingular, the problem (B.1) is *regular*, and the matrices $\boldsymbol{\Delta}_0^{-1} \boldsymbol{\Delta}_1, \ldots, \boldsymbol{\Delta}_0^{-1} \boldsymbol{\Delta}_r$ commute. A regular *r*-parameter eigenvalue problem (B.1) has $\prod_{i=1}^r n_i$ eigenvalues.

Example 1. For $r = 2$, the problem (B.1) has the form

$$\mathbf{A}_{10} \mathbf{x}_1 + \lambda_1 \mathbf{A}_{11} \mathbf{x}_1 + \lambda_2 \mathbf{A}_{12} \mathbf{x}_1 = \mathbf{0}, \tag{B.5a}$$

$$\mathbf{A}_{20} \mathbf{x}_2 + \lambda_1 \mathbf{A}_{21} \mathbf{x}_2 + \lambda_2 \mathbf{A}_{22} \mathbf{x}_2 = \mathbf{0}. \tag{B.5b}$$

If we multiply (B.5a) by $\mathbf{A}_{22} \mathbf{x}_2$ from the right and multiply (B.5b) by $\mathbf{A}_{12} \mathbf{x}_1$ from the left using the Kronecker product, we obtain

$$(\mathbf{A}_{10} \otimes \mathbf{A}_{22})(\mathbf{x}_1 \otimes \mathbf{x}_2) + \lambda_1 (\mathbf{A}_{11} \otimes \mathbf{A}_{22})(\mathbf{x}_1 \otimes \mathbf{x}_2) + \lambda_2 (\mathbf{A}_{12} \otimes \mathbf{A}_{22})(\mathbf{x}_1 \otimes \mathbf{x}_2) = \mathbf{0}, \tag{B.6a}$$

$$(\mathbf{A}_{12} \otimes \mathbf{A}_{20})(\mathbf{x}_1 \otimes \mathbf{x}_2) + \lambda_1 (\mathbf{A}_{12} \otimes \mathbf{A}_{21})(\mathbf{x}_1 \otimes \mathbf{x}_2) + \lambda_2 (\mathbf{A}_{12} \otimes \mathbf{A}_{22})(\mathbf{x}_1 \otimes \mathbf{x}_2) = \mathbf{0}. \tag{B.6b}$$

Taking $\mathbf{z} = \mathbf{x}_1 \otimes \mathbf{x}_2$ and subtracting (B.6b) from (B.6a) yields the generalized eigenvalue problem

$$(\mathbf{A}_{12} \otimes \mathbf{A}_{20} - \mathbf{A}_{10} \otimes \mathbf{A}_{22})\mathbf{z} = \lambda_1 (\mathbf{A}_{11} \otimes \mathbf{A}_{22} - \mathbf{A}_{12} \otimes \mathbf{A}_{21})\mathbf{z}. \tag{B.7}$$

In a similar way, we obtain from (B.5) the second generalized eigenvalue problem

$$(\mathbf{A}_{10} \otimes \mathbf{A}_{21} - \mathbf{A}_{11} \otimes \mathbf{A}_{20})\mathbf{z} = \lambda_2 (\mathbf{A}_{11} \otimes \mathbf{A}_{22} - \mathbf{A}_{12} \otimes \mathbf{A}_{21})\mathbf{z}. \tag{B.8}$$

From (B.3) and (B.4), we can write (B.7) and (B.8) as $\boldsymbol{\Delta}_1 \mathbf{z} = \lambda_1 \boldsymbol{\Delta}_0 \mathbf{z}$ and $\boldsymbol{\Delta}_2 \mathbf{z} = \lambda_2 \boldsymbol{\Delta}_0 \mathbf{z}$, which is equal to (B.2).

Appendix C. Apply shift to singular problem

The matrices $\boldsymbol{\Delta}_i$, $i = 0, \ldots, 4$, associated with the four-parameter eigenvalue problem (43) are such that $\boldsymbol{\Delta}_0$ is singular, but $\boldsymbol{\Delta}_0 + s \boldsymbol{\Delta}_4$ is nonsingular for a generic shift $s \neq 0$. Thus, it is more efficient to solve a shifted system of generalized eigenvalue problems

$$\boldsymbol{\Delta}_1 \mathbf{z} = \mathrm{i}\widetilde{k}(\boldsymbol{\Delta}_0 + s \boldsymbol{\Delta}_4)\mathbf{z}, \quad \boldsymbol{\Delta}_2 \mathbf{z} = \mathrm{i}\widetilde{\kappa}_{y,1}(\boldsymbol{\Delta}_0 + s \boldsymbol{\Delta}_4)\mathbf{z}, \quad \boldsymbol{\Delta}_3 \mathbf{z} = \mathrm{i}\widetilde{\kappa}_{y,2}(\boldsymbol{\Delta}_0 + s \boldsymbol{\Delta}_4)\mathbf{z}, \quad \boldsymbol{\Delta}_4 \mathbf{z} = \widetilde{\xi}_0(\boldsymbol{\Delta}_0 + s \boldsymbol{\Delta}_4)\mathbf{z} \tag{C.1}$$

and then recover the eigenvalues of (43) as

$$\mathrm{i}k = \frac{\mathrm{i}\widetilde{k}}{1 - s\widetilde{\xi}_0}, \quad \mathrm{i}\kappa_{y,1} = \frac{\mathrm{i}\widetilde{\kappa}_{y,1}}{1 - s\widetilde{\xi}_0}, \quad \mathrm{i}\kappa_{y,2} = \frac{\mathrm{i}\widetilde{\kappa}_{y,2}}{1 - s\widetilde{\xi}_0}, \quad \xi_0 = \frac{\widetilde{\xi}_0}{1 - s\widetilde{\xi}_0}. \tag{C.2}$$

This approach circumvents the computationally complex staircase algorithm. Note that the infinite eigenvalues of (43) correspond to $1 - s\widetilde{\xi}_0 = 0$. The same idea can be applied to (46), where $\boldsymbol{\Delta}_0 + s \boldsymbol{\Delta}_6$ is nonsingular for a generic shift $s \neq 0$.

---

[8] The Kronecker product $\mathbf{A} \otimes \mathbf{B}$ of the $m \times n$-matrix $\mathbf{A} = [A_{ij}]$ with the $p \times q$-matrix $\mathbf{B}$ yields the block matrix $[A_{ij}\mathbf{B}]$ of size $mp \times nq$. For three matrices, $\mathbf{A} \otimes \mathbf{B} \otimes \mathbf{C} = (\mathbf{A} \otimes \mathbf{B}) \otimes \mathbf{C} = \mathbf{A} \otimes (\mathbf{B} \otimes \mathbf{C})$. Vectors are treated like matrices with one column. For two matrices and two vectors, $(\mathbf{Ax}) \otimes (\mathbf{By}) = (\mathbf{A} \otimes \mathbf{B})(\mathbf{x} \otimes \mathbf{y})$.

Appendix D. Improve efficiency for isotropic plates

The quadratic eigenvalue problem (7) describing the free plate is typically solved at a given frequency by employing a linearization, resulting in a standard eigenvalue problem of twice the original size in k. If the plate consists of isotropic materials, there exists a transformation yielding a linear eigenvalue problem *of the original size*. That is to say, it involves terms multiplied by k^2 but none in k so that we can treat it as a linear eigenvalue problem in $\xi_0 = -k^2$. If the isotropic plate is coupled to unbounded fluid media, we can apply this approach analogously to our current formulation after minor modifications concerning the interface conditions. Consider the problem (43) and sort the degrees of freedom into horizontal displacements, vertical displacements, and pressures. As is known in the case of free plates [65,67], the resulting finite-element matrices have a particular block structure:

$$
\left(-\begin{bmatrix} \overline{\mathbf{E}}_2^{xx} & \mathbf{0} & \mathbf{0} \\ \mathbf{0} & \overline{\mathbf{E}}_2^{yy} & \overline{\mathbf{E}}_2^{yp} \\ \mathbf{0} & \mathbf{0} & \mathbf{0} \end{bmatrix} + \omega^2 \begin{bmatrix} \overline{\mathbf{M}}^{xx} & \mathbf{0} & \mathbf{0} \\ \mathbf{0} & \overline{\mathbf{M}}^{yy} & \mathbf{0} \\ \mathbf{0} & \overline{\mathbf{M}}^{py} & \mathbf{0} \end{bmatrix} + \mathrm{i}k \begin{bmatrix} \mathbf{0} & \overline{\mathbf{E}}_1^{xy} & \mathbf{0} \\ \overline{\mathbf{E}}_1^{yx} & \mathbf{0} & \mathbf{0} \\ \mathbf{0} & \mathbf{0} & \mathbf{0} \end{bmatrix} + (\mathrm{i}k)^2 \begin{bmatrix} \overline{\mathbf{E}}_0^{xx} & \mathbf{0} & \mathbf{0} \\ \mathbf{0} & \overline{\mathbf{E}}_0^{yy} & \mathbf{0} \\ \mathbf{0} & \mathbf{0} & \mathbf{0} \end{bmatrix} \right.
$$
$$
\left. + \mathrm{i}\kappa_{y,1} \begin{bmatrix} \mathbf{0} & \mathbf{0} & \mathbf{0} \\ \mathbf{0} & \mathbf{0} & \mathbf{0} \\ \mathbf{0} & \mathbf{0} & \mathbf{R}_1^{pp} \end{bmatrix} + \mathrm{i}\kappa_{y,2} \begin{bmatrix} \mathbf{0} & \mathbf{0} & \mathbf{0} \\ \mathbf{0} & \mathbf{0} & \mathbf{0} \\ \mathbf{0} & \mathbf{0} & \mathbf{R}_2^{pp} \end{bmatrix} \right) \begin{bmatrix} \mathbf{u}_n^x \\ \mathbf{u}_n^y \\ \mathbf{p}_n \end{bmatrix} = \mathbf{0}. \tag{D.1}
$$

We multiply the second and third equations in the above system by $\mathrm{i}k$ and modify the eigenvectors to obtain

$$
\left(-\begin{bmatrix} \overline{\mathbf{E}}_2^{xx} & -\overline{\mathbf{E}}_1^{xy} & \mathbf{0} \\ \mathbf{0} & \overline{\mathbf{E}}_2^{yy} & \overline{\mathbf{E}}_2^{yp} \\ \mathbf{0} & \mathbf{0} & \mathbf{0} \end{bmatrix} + \omega^2 \begin{bmatrix} \overline{\mathbf{M}}^{xx} & \mathbf{0} & \mathbf{0} \\ \mathbf{0} & \overline{\mathbf{M}}^{yy} & \mathbf{0} \\ \mathbf{0} & \overline{\mathbf{M}}^{py} & \mathbf{0} \end{bmatrix} + (\mathrm{i}k)^2 \begin{bmatrix} \overline{\mathbf{E}}_0^{xx} & \mathbf{0} & \mathbf{0} \\ \overline{\mathbf{E}}_1^{yx} & \overline{\mathbf{E}}_0^{yy} & \mathbf{0} \\ \mathbf{0} & \mathbf{0} & \mathbf{0} \end{bmatrix} \right.
$$
$$
\left. + \mathrm{i}\kappa_{y,1} \begin{bmatrix} \mathbf{0} & \mathbf{0} & \mathbf{0} \\ \mathbf{0} & \mathbf{0} & \mathbf{0} \\ \mathbf{0} & \mathbf{0} & \mathbf{R}_1^{pp} \end{bmatrix} + \mathrm{i}\kappa_{y,2} \begin{bmatrix} \mathbf{0} & \mathbf{0} & \mathbf{0} \\ \mathbf{0} & \mathbf{0} & \mathbf{0} \\ \mathbf{0} & \mathbf{0} & \mathbf{R}_2^{pp} \end{bmatrix} \right) \begin{bmatrix} \mathbf{u}_n^x \\ \mathrm{i}k\,\mathbf{u}_n^y \\ \mathrm{i}k\,\mathbf{p}_n \end{bmatrix} = \mathbf{0}. \tag{D.2}
$$

Hence, we have obtained a three-parameter eigenvalue problem with parameters $\mathrm{i}\kappa_{y,1}$, $\mathrm{i}\kappa_{y,2}$, ξ_0 that is solved analogously to (43) but without requiring (43d). Consequently, the operator determinants are of size $4n_1 \times 4n_1$ (instead of $8n_1 \times 8n_1$), leading to a less expensive assembly and solution of the generalized eigenproblem (B.2).

References

[1] L.M. Flitman, On the motion of a rigid strip-mass lying on an elastic half-space and excited by a seismic wave, J. Appl. Math. Mech. 26 (6) (1962) 1043–1058, http://dx.doi.org/10.1016/0021-8928(62)90194-6.

[2] E. Kausel, J.M. de Oliveira Barbosa, Analysis of embankment underlain by elastic half-space: 2.5D model with paralongitudinal approximations to the half-space, Soil Dyn. Earthq. Eng. 155 (2022) 107090, http://dx.doi.org/10.1016/j.soildyn.2021.107090.

[3] B.W. Drinkwater, M. Castaings, B. Hosten, The interaction of Lamb waves with solid-solid interfaces, in: Rev. Prog. Quant. Nondestruct. Eval., Vol. 22, 2003, pp. 1064–1071.

[4] A. Pelat, S. Felix, V. Pagneux, A coupled modal-finite element method for the wave propagation modeling in irregular open waveguides, J. Acoust. Soc. Am. 129 (3) (2011) 1240–1249, http://dx.doi.org/10.1121/1.3531928.

[5] E. Pistone, P. Rizzo, On the use of an array of ultrasonic immersion transducers for the nondestructive testing of immersed plates, Nondestruct. Test. Eval. 30 (1) (2015) 26–38, http://dx.doi.org/10.1080/10589759.2014.979817.

[6] H. Lamb, On waves in an elastic plate, Proc. R. Soc. Lond. 93 (648) (1917) 114–128, http://dx.doi.org/10.1098/rspa.1917.0008.

[7] E. Kausel, Lamb's problem at its simplest, Proc. R. Soc. A 469 (2013) 20120462, http://dx.doi.org/10.1098/rspa.2012.0462.

[8] L. Knopoff, A matrix method for elastic wave problems, Bull. Seismol. Soc. Am. 54 (1) (1964) 431–438, http://dx.doi.org/10.1785/bssa0540010431.

[9] A.H. Nayfeh, The general problem of elastic wave propagation in multilayered anisotropic media, J. Acoust. Soc. Am. 89 (4) (1991) 1521–1531, http://dx.doi.org/10.1121/1.400988.

[10] A.M.A. Huber, Classification of solutions for guided waves in fluid-loaded viscoelastic composites with large numbers of layers, J. Acoust. Soc. Am. 154 (2) (2023) 1073–1094, http://dx.doi.org/10.1121/10.0020584.

[11] R.B. Nelson, On natural vibrations and waves in laminated orthotropic plates, J. Appl. Mech. (1972) 739–745.

[12] E. Kausel, J.M. Roësset, Semianalytic hyperelement for layered strata, J. Eng. Mech. Div. 103 (4) (1977) 569–588, http://dx.doi.org/10.1061/jmcea3.0002251.

[13] I. Bartoli, A. Marzani, F. Lanza di Scalea, E. Viola, Modeling wave propagation in damped waveguides of arbitrary cross-section, J. Sound Vib. 295 (2006) 685–707, http://dx.doi.org/10.1016/j.jsv.2006.01.021.

[14] H. Gravenkamp, C. Song, J. Prager, A numerical approach for the computation of dispersion relations for plate structures using the scaled boundary finite element method, J. Sound Vib. 331 (2012) 2543–2557, http://dx.doi.org/10.1016/j.jsv.2012.01.029.

[15] H. Gravenkamp, S. Natarajan, W. Dornisch, On the use of NURBS-based discretizations in the scaled boundary finite element method for wave propagation problems, Comput. Methods Appl. Mech. Engrg. 315 (2017) 867–880, http://dx.doi.org/10.1016/j.cma.2016.11.030.

[16] D.A. Kiefer, B. Plestenjak, H. Gravenkamp, C. Prada, Computing zero-group-velocity points in anisotropic elastic waveguides: globally and locally convergent methods, J. Acoust. Soc. Am. 153 (2) (2023) 1386–1398.

[17] E. Kausel, Accurate stresses in the thin-layer method, Internat. J. Numer. Methods Engrg. 61 (2004) 360–379, http://dx.doi.org/10.1002/nme.1067.

[18] M. Mazzotti, I. Bartoli, A. Marzani, E. Viola, A coupled SAFE-2.5D BEM approach for the dispersion analysis of damped leaky guided waves in embedded waveguides of arbitrary cross-section., Ultrasonics 53 (7) (2013) 1227–1241, http://dx.doi.org/10.1016/j.ultras.2013.03.003.

[19] C. Song, J.P. Wolf, The scaled boundary finite-element method — alias consistent infinitesimal finite-element cell method — for elastodynamics, Comput. Methods Appl. Mech. Engrg. 147 (1997) 329–355, http://dx.doi.org/10.1016/S0045-7825(97)00021-2.

[20] H. Gravenkamp, C. Birk, C. Song, Simulation of elastic guided waves interacting with defects in arbitrarily long structures using the scaled boundary finite element method, J. Comput. Phys. 295 (2015) 438–455, http://dx.doi.org/10.1016/j.jcp.2015.04.032.

[21] F. Krome, H. Gravenkamp, A semi-analytical curved element for linear elasticity based on the scaled boundary finite element method, Internat. J. Numer. Methods Engrg. 109 (2017) 790–808, http://dx.doi.org/10.1002/nme.5306.

[22] M. Castaings, M.J.S. Lowe, Finite element model for waves guided along solid systems of arbitrary section coupled to infinite solid media, J. Acoust. Soc. Am. 123 (2) (2008) 696–708, http://dx.doi.org/10.1121/1.2821973.

[23] F. Treyssède, K.L. Nguyen, A.-S. Bonnet-Bendhia, C. Hazard, On the use of a SAFE-PML technique for modeling two-dimensional open elastic waveguides, in: Acoustics, 2012, pp. 1–6.

[24] K.L. Nguyen, F. Treyssède, A.-S. Bonnet-Bendhia, C. Hazard, Computation of dispersion curves in elastic waveguides of arbitrary cross-section embedded in infinite solid media, in: Int. Symp. Nondestruct. Charact. Mater., 2013, pp. 1–8.

[25] J.-P. Berenger, A perfectly matched layer for the absorption of electromagnetic waves, J. Comput. Phys. 114 (2) (1994) 185–200, http://dx.doi.org/10.1006/jcph.1994.1159.

[26] X. Qi, X. Zhao, Guided wave propagation in solid structures of arbitrary crosssection coupled to infinite media, AIP Conf. Proc. 1681 (2010) 1681–1688, http://dx.doi.org/10.1063/1.3362269.

[27] H. Jia, M.M. Jing, L.R. Joseph, J.L. Rose, Guided wave propagation in single and double layer hollow cylinders embedded in infinite media, J. Acoust. Soc. Am. 129 (2) (2011) 691–700, http://dx.doi.org/10.1121/1.3531807.

[28] E. Georgiades, M.J.S. Lowe, R.V. Craster, Leaky wave characterisation using spectral methods, J. Acoust. Soc. Am. 152 (3) (2022) 1487–1497, http://dx.doi.org/10.1121/10.0013897.

[29] E. Georgiades, M.J.S. Lowe, R.V. Craster, Computing leaky Lamb waves for waveguides between elastic half-spaces using spectral collocation, J. Acoust. Soc. Am. 155 (1) (2024) 629–639, http://dx.doi.org/10.1121/10.0024467.

[30] H. Gravenkamp, C. Birk, C. Song, Computation of dispersion curves for embedded waveguides using a dashpot boundary condition, J. Acoust. Soc. Am. 135 (3) (2014) 1127–1138, http://dx.doi.org/10.1121/1.4864303.

[31] H. Gravenkamp, C. Birk, J. Van, Modeling ultrasonic waves in elastic waveguides of arbitrary cross-section embedded in infinite solid medium, Comput. Struct. 149 (2015) 61–71, http://dx.doi.org/10.1016/j.compstruc.2014.11.007.

[32] H. Gravenkamp, C. Birk, C. Song, Numerical modeling of elastic waveguides coupled to infinite fluid media using exact boundary conditions, Comput. Struct. 141 (2014) 36–45, http://dx.doi.org/10.1016/j.compstruc.2014.05.010.

[33] D.A. Kiefer, M. Ponschab, S.J. Rupitsch, M. Mayle, Calculating the full leaky Lamb wave spectrum with exact fluid interaction, J. Acoust. Soc. Am. 145 (6) (2019) 3341–3350, http://dx.doi.org/10.1121/1.5109399.

[34] D.A. Kiefer, Elastodynamic quasi-guided waves for transit-time ultrasonic flow metering, in: FAU Forschungen, Reihe B, Medizin, Naturwissenschaft, Technik, no. 42, FAU University Press, Erlangen, 2022, http://dx.doi.org/10.25593/978-3-96147-550-6.

[35] T. Hayashi, D. Inoue, Calculation of leaky Lamb waves with a semi-analytical finite element method, Ultrasonics 54 (2014) 1460–1469, http://dx.doi.org/10.1016/j.ultras.2014.04.021, arXiv:24838216.

[36] S. Tang, J. Yin, C. Wang, G. Zhu, Study on leaky Lamb waves in functionally graded composites loaded by asymmetric fluids, Waves Random Complex Media 1 (2022) 1–20, http://dx.doi.org/10.1080/17455030.2022.2102270.

[37] E. Ducasse, M. Deschamps, Mode computation of immersed multilayer plates by solving an eigenvalue problem, Wave Motion 112 (2022) 102962, http://dx.doi.org/10.1016/j.wavemoti.2022.102962.

[38] H. Gravenkamp, F. Bause, C. Song, On the computation of dispersion curves for axisymmetric elastic waveguides using the Scaled Boundary Finite Element Method, Comput. Struct. 131 (2014) 46–55, http://dx.doi.org/10.1016/j.compstruc.2013.10.014.

[39] V. Mehrmann, H. Voss, Nonlinear eigenvalue problems: a challenge for modern eigenvalue methods, GAMM-Mitt. 27 (2004) 121–152, http://dx.doi.org/10.1002/gamm.201490007.

[40] S. Güttel, F. Tisseur, The nonlinear eigenvalue problem, Acta Numer. 26 (2017) 1–94, http://dx.doi.org/10.1017/S0962492917000034.

[41] E. Jarlebring, G. Mele, O. Runborg, The waveguide eigenvalue problem and the tensor infinite Arnoldi method, SIAM J. Sci. Comput. 39 (2017) A1062–A1088, http://dx.doi.org/10.1137/15M10446.

[42] C. Campos, J.E. Roman, NEP: a module for the parallel solution of nonlinear eigenvalue problems in SLEPc, ACM Trans. Math. Software 47 (3) (2021) 1–29, http://dx.doi.org/10.1145/3447544.

[43] E. Ringh, E. Jarlebring, Nonlinearizing two-parameter eigenvalue problems, SIAM J. Matrix Anal. Appl. 42 (2) (2021) 775–799, http://dx.doi.org/10.1137/19M1274316.

[44] F.V. Atkinson, A.B. Mingarelli, Multiparameter Eigenvalue Problems, CRC Press, Boca Raton, FL, 2011, p. xviii+283, Sturm-Liouville theory.

[45] B. Plestenjak, C.I. Gheorghiu, M.E. Hochstenbach, Spectral collocation for multiparameter eigenvalue problems arising from separable boundary value problems, J. Comput. Phys. 298 (2015) 585–601, http://dx.doi.org/10.1016/j.jcp.2015.06.015.

[46] M.E. Hochstenbach, T. Košir, B. Plestenjak, A Jacobi–Davidson type method for the two-parameter eigenvalue problem, SIAM J. Matrix Anal. Appl. 26 (2) (2004) 477–497, http://dx.doi.org/10.1137/S0895479802418318.

[47] A. Muhič, B. Plestenjak, On the quadratic two-parameter eigenvalue problem and its linearization, Linear Algebra Appl. 432 (10) (2010) 2529–2542, http://dx.doi.org/10.1016/j.laa.2009.12.022.

[48] B. Plestenjak, MultiParEig (version 2.7.0.0), 2023, MATLAB Central File Exchange. URL www.mathworks.com/matlabcentral/fileexchange/47844-multipareig.

[49] H. Gravenkamp, B. Plestenjak, D.A. Kiefer, E. Jarlebring, Leaky Guided Waves Examples (version 1.0.0), 2024, http://dx.doi.org/10.5281/zenodo.13825263, URL https://github.com/haukegravenkamp/Leaky-Guided-Waves-Examples.

[50] H. Gravenkamp, SAMWISE - Semi-Analytical Modeling of Waves in Structural Elements (version 1.0.0), 2024, http://dx.doi.org/10.5281/zenodo.13830671, URL https://github.com/haukegravenkamp/SAMWISE.

[51] D.A. Kiefer, GEWtool, 2023, http://dx.doi.org/10.5281/zenodo.10114243, URL https://github.com/dakiefer/GEWtool.

[52] O.C. Zienkiewicz, R.L. Taylor, J.Z. Zhu, The Finite Element Method: Its Basis & Fundamentals, fifth ed., Butterworth Heinemann, 2013.

[53] E. Kausel, Wave propagation in anisotropic layered media, Internat. J. Numer. Methods Engrg. 23 (1986) 1567–1578, http://dx.doi.org/10.1002/nme.1620230811.

[54] H. Gravenkamp, H. Man, C. Song, J. Prager, The computation of dispersion relations for three-dimensional elastic waveguides using the Scaled Boundary Finite Element Method, J. Sound Vib. 332 (2013) 3756–3771, http://dx.doi.org/10.1016/j.jsv.2013.02.007.

[55] H. Gravenkamp, A. Saputra, S. Duczek, High-order shape functions in the Scaled Boundary Finite Element Method revisited, Arch. Comput. Methods Eng. 28 (2021) 473–494, http://dx.doi.org/10.1007/s11831-019-09385-1.

[56] E.M. Viggen, H.K. Arnestad, Modelling acoustic radiation from vibrating surfaces around coincidence: Radiation into fluids, J. Sound Vib. 560 (2023) 117787, http://dx.doi.org/10.1016/j.jsv.2023.117787.

[57] N.F. Declercq, R. Briers, J. Degrieck, O. Leroy, The history and properties of ultrasonic inhomogeneous waves, IEEE Trans. Ultrason. Ferroelectr. Freq. Control 52 (5) (2005) 776–791, http://dx.doi.org/10.1109/TUFFC.2005.1503963.

[58] J.L. Rose, Ultrasonic Waves in Solid Media, first ed., Cambridge University Press, 1999.

[59] E. Kausel, Fundamental Solutions in Elastodynamics, first ed., Cambridge University Press, 2006.

[60] B. Pavlakovic, M.J.S. Lowe, Disperse (version 2.0.16i), 2011, URL www.disperse.software.

[61] B. Pavlakovic, M.J.S. Lowe, D.N. Alleyne, Disperse: A general purpose program for creating dispersion curves, in: Rev. Prog. Quant. NDE, Plenum Press, 1997, pp. 185–192, http://dx.doi.org/10.1007/978-1-4615-5947-4_24.

[62] K.-J. Langenberg, R. Marklein, K. Mayer, Ultrasonic Nondestructive Testing of Materials, first ed., CRC Press, 2012, http://dx.doi.org/10.1201/b11724.

[63] H. Gravenkamp, C. Birk, C. Song, The computation of dispersion relations for axisymmetric waveguides using the Scaled Boundary Finite Element Method, Ultrasonics 54 (2014) 1373–1385, http://dx.doi.org/10.1016/j.ultras.2014.02.004.

[64] H. Gravenkamp, Numerical Methods for the Simulation of Ultrasonic Guided Waves (Ph.D. thesis), TU Braunschweig, 2014.

[65] H. Gravenkamp, Efficient simulation of elastic guided waves interacting with notches, adhesive joints, delaminations and inclined edges in plate structures, Ultrasonics 82 (2018) 101–113, http://dx.doi.org/10.1016/j.ultras.2017.07.019.

[66] F.V. Atkinson, Multiparameter Eigenvalue Problems, in: Mathematics in Science and Engineering, Vol. 82, Matrices and compact operators, Academic Press, New York-London, 1972, p. xii+209, Volume I.

[67] E. Kausel, An Explicit Solution for the Green Functions for Dynamic Loads in Layered Media, vol. R81-13, Massachusetts Institute of Technology, 1981.